Estimating bedload transport rates in a gravel-bed river using seismic impact plates: model development and application

Philip J. Soar[1] and Peter W. Downs[2]

[1] Department of Geography, University of Portsmouth, Buckingham Building, Lion Terrace, Portsmouth PO1 3HE, U.K.

philip.soar@port.ac.uk (corresponding author)

+44(0)23 9284 2482

[2] School of Geography, Earth and Environmental Sciences, Portland Square, Drake Circus, Plymouth University, Plymouth PL4 8AA, U.K.

peter.downs@plymouth.ac.uk

+44(0)1752 584990

Abstract

A data-driven, uncertainty-bound estimation technique for bedload transport rates is developed based on passive sensing devices. The model converts sediment samples to a mass in transit for each instantaneous discharge according to impacts detected and a Monte Carlo simulation of the load determined at random from the particle size distribution. Using impact count data autogenically produces a supply-limited, location-specific and high-resolution time-series of bedload rates, while the probabilistic approach inherently accommodates the stochastic nature of bedload transport. Application to the River Avon (Devon, U.K.) provides cross-sectional bedload rate estimates within the bounds of experimental data and calibrated to observed field behaviour. This new procedure offers an alternative 'class' of bedload estimation to existing approaches and has the potential for wide-ranging applications in river management and restoration, while contributing to the integration of 'big data' into a progressive agenda for hydrogeomorphology research.

Keywords

Coarse bedload transport; Fluvial geomorphology; Monte Carlo simulation; Sediment monitoring; Seismic impact plate; Uncertainty

Software Availability

Name of model: Bedload from Impact Plates (BLIP)

Developers: Philip Soar, University of Portsmouth, U.K. (philip.soar@port.ac.uk); Peter Downs, Plymouth University, U.K. (peter.downs@plymouth.ac.uk)

Program language: Visual Basic for Applications (VBA)

Hardware required: Microsoft Windows PC

Software required: Microsoft Excel

Availability: A working model has been developed and is proposed for general release in the near future. The model can be made available to researchers on request to the authors

1. Introduction

Fluvial system sciences have seen the enthusiastic uptake of 'big data' over recent decades, with high-resolution, passively-sensed data sets becoming integral both to spatial analyses of terrain and to time-series investigations of water quality and suspended sediment transport. One outstanding challenge is the adequate characterization and prediction of bedload, with technological innovation considered the catalyst to developing detailed insights into transport processes (Ashmore and Rennie, 2012) that are critical to better understand physical habitat dynamics, underpin sustainable flood risk management and ensure the resilience of river restoration schemes.

Active, direct measurement of bedload using samplers or traps (Bunte et al., 2004, 2008) are costly in terms of labour (portable samplers) and/or infrastructure (permanent installations), logistically challenging to achieve with acceptable accuracy over geomorphologically-relevant time periods (Ryan and Porth, 1999; Sterling and Church, 2002; Vericat et al., 2006) and often involve hazardous working conditions. Alternatively, transport rates are estimated using empirical formulae, although such methods are characterized by marked differences in performance (e.g. Barry et al., 2004; Gomez and Church, 1989; Martin and Ham, 2005; Wilcock, 2001) arising from the computational simplifications required to represent the complex physics of bedload movement in a practicable manner. In particular, these numerical expressions cannot account for the inherently stochastic nature of bedload transport (see Recking et al., 2012) and are incapable of capturing intra- and inter-event variations in supply (Gomez, 2006). Sediment routing models and mobile boundary simulations (Bruner and Gibson, 2005; Cui et al., 2011; Papanicolaou et al., 2008) offer the potential to overcome some of these issues but are currently extremely difficult to set up and parameterize (except by an experienced modeller) and are rarely validated in practice (Thorne et al., 2011; Wallerstein et al., 2006). Recognizing the difficulties and limitations of direct measurement and unreliability of sediment transport equations, Wilcock (2001) appealed for new methods to be sought that strike a balance between accuracy and practicability.

Passive approaches to bedload monitoring are centred on recording the passage of bedload using an acoustic or seismic sensor that records an electrical wave (hydrophones, geophones, respectively) or simply an impulse (impact plates) as particles pass or strike the sensor. Modern data loggers provide a means of obtaining high-resolution spatial and temporal measurement of coarse bedload transport intensity over time periods of geomorphological relevance (Gray et al., 2010a). Such devices are relatively low cost (e.g. USD 900 per plate for those used here), portable and non-intrusive and, as a passive technique, offer far safer data collection. Depending on the sensor used, the minimum particle size recorded is usually in the range of 4 to 30 mm (Gray et al., 2010b; Rickenmann et al., 2012). There is a rapidly growing body of literature associated with these devices (summaries in Gray et al., 2010a, b; Rickenmann, in press; Rickenmann et al., 2014), and an evolving understanding of their performance characteristics in relation to experimental set-up, grain-size dependent and transport-style effects (Beylich and Laute, 2014; Gray et al., 2010b; Rickenmann and Fritschi, 2010; Rickenmann and McArdell, 2007, 2008; Rickenmann et al., 2012, 2014; Tsakiris et al., 2014; Turowski and Rickenmann, 2009; Wyss et al., 2016a, 2016b, 2016c) and the dynamics of sediment supply during individual events (Downs et al., 2016).

There is now growing evidence for a robust correlation between summed impact counts and total bedload mass over event-scale and longer time periods (Beylich and Laute, 2014; Rickenmann et al., 2012, 2014). However, a significant question concerns the calibration of passive devices to convert data collected on bedload transport *intensity* into estimates of bedload transport *rates* (see review by Rickenmann, in press). Research focussed initially on direct calibration of either summed impulse counts or a summary measure of acoustic signal against a measured sediment load to produce a rating curve but has more recently centred on extracting grain size information from the acoustic signal (Barrière et al., 2015; Bogen and Møen, 2003; Møen et al., 2010; Rickenmann et al., 2014; Wyss et al., 2014, 2016b) and correlating the signal strength to bedload transport rate as a function of sediment grain size (Wyss et al., 2016a). While acoustic fingerprinting techniques offer considerable promise for reconstructing continuous rates of bedload transport by size fraction, the approach is subject to time-consuming direct measurements (Turowski and Rickenmann, 2011), may require a lengthy refinement period and cannot facilitate rate estimates to be derived in the vast majority of rivers where bedload monitoring is not undertaken routinely. As such, environmental managers cannot as yet benefit from the 'revolutionary' potential afforded to bedload understanding from passive sensors (Gray et al., 2010b).

Addressing this issue, we focus here on a complementary, indirect, approach for estimating bedload transport rates probabilistically from bedload counts detected by seismic impact plates using a Monte Carlo simulation in conjunction with knowledge of particle size distribution of bed material and parameters of the flow and cross-sectional geometry. The approach offers the prospect of developing new insights into bedload transport dynamics while also enabling sensitivity testing and scenario-modelling of future conditions. We illustrate the method with application to a gravel-bed river in South West England during an extremely wet year, building on the insights offered from the impact count data alone (Downs et al., 2016). Without the need for permanent bedload monitoring infrastructure, this new procedure thus provides a potentially robust method of achieving indicative measures of bedload transport load for wide-ranging practical applications and in so doing affords one means of fulfilling the revolutionary potential of passive sensors in fluvial sedimentology.

2. Model Development

2.1 Model overview

The overarching assumption of the model is that in gravel-bed streams with variable sizes of bed material, impacts detected by a seismic plate are generated by a probabilistic array of 'possible' particle sizes in transit that reflects a proportion of the distribution of bed material grain sizes, constrained by a minimum size detectable by the equipment and a maximum size at the threshold for bedload motion.

The process for generating cross-sectional sediment rates from impact plate count data consists of four principal stages, illustrated in Figure 1 and discussed below. Experimentally, the approach requires deployment of a cross-sectional array of impact plates in conjunction with one or more pressure transducers. As depth of flow is a critical parameter in the model, deployment of a pressure transducer as a component of the experimental set-up is essential and, therefore, it is recommended investigators consider strongly the deployment of two or more pressure transducers to facilitate logging of water surface slope. While a single impact plate can be used to explore temporal patterns of bedload occurring at or near the thalweg, sediment paths have been found to shift markedly with discharge (Downs et al., 2016). Therefore, resources permitting, multiple plate deployment across a section is recommended to better represent the natural spatio-temporal variation in sediment transport intensity over the channel bed and should improve accuracy. The discernible improvement in accuracy of empirical methods of transport rate estimation with increasing number of samples taken, and beneficial performance over sediment transport formulae, is illustrated for gravel-bed rivers by Wilcock (2001).

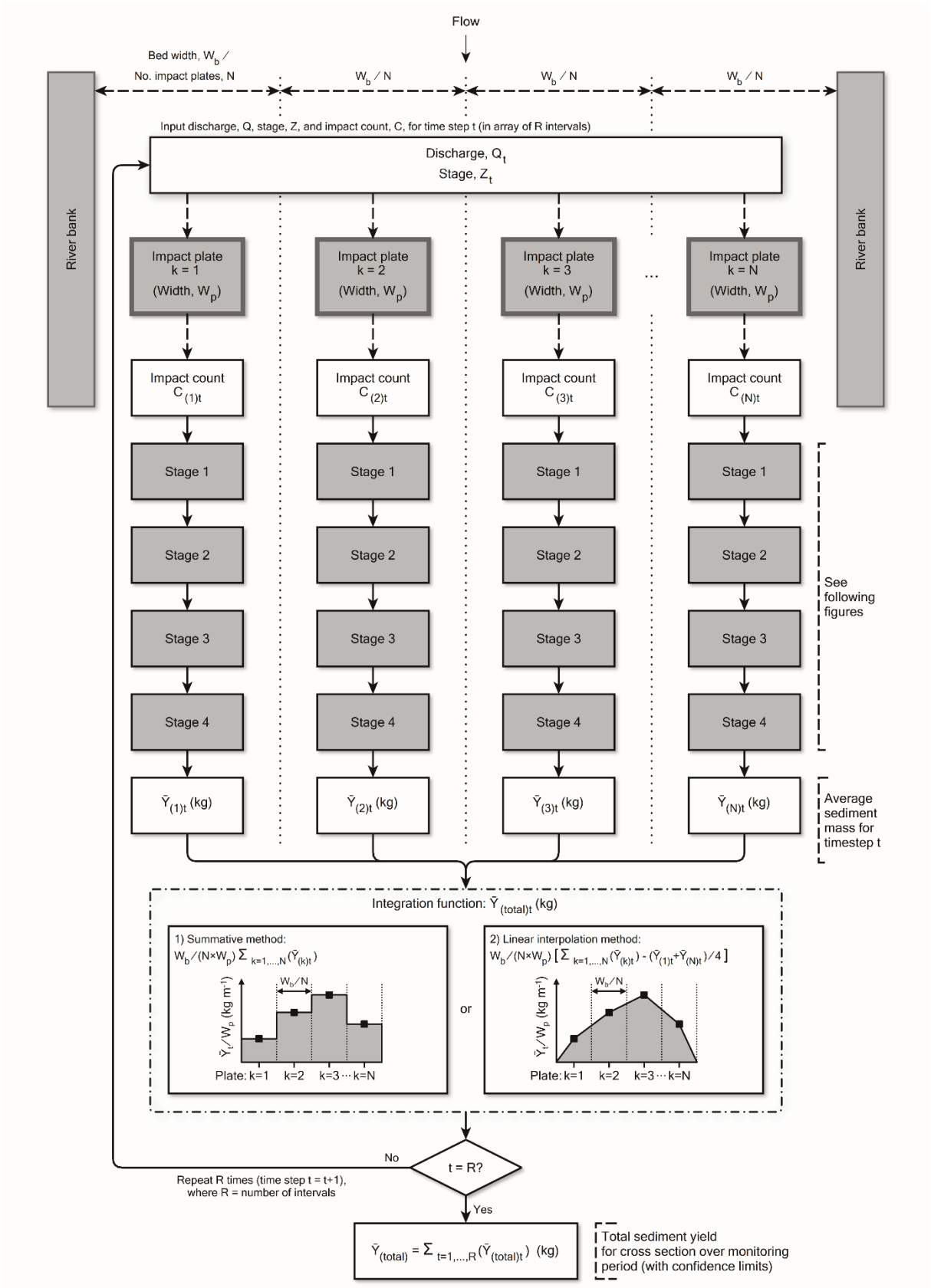

Fig. 1. Stages involved in generating probabilistic cross-sectional bedload yield using the 'Bedload from Impact Plates' (BLIP) model (see text for details).

Measurements made at each time step (t) in the time-series of impact counts thus comprise: the number of bedload impacts detected (count, C); water surface elevation (stage, Z), and; water surface slope (S). Discharge (Q) is not used directly in the model as the conversion of impacts to transport rates is a function of water depth, however a corresponding time series of discharge is critical for exploring relationships between derived bedload rate and flow. At ungauged sites, discharge can be simulated from the Manning equation (or alternative flow resistance equation) or if fortunate to be reasonably close to a gauging station, discharge can be extracted from the gauge record.

The working model 'Bedload from Impact Plates' (BLIP) is coded in VBA and integrates with field data tabulated in MS Excel. The model assumes a series of N impact plates are sited across the channel bed width (W_b) in the middle of equally spaced bed segments of width W_b/N. For each measurement time step (t), discharge, stage and water surface slope are updated and the model progresses through the four stages to convert impact counts ($C_{(k)t}$) to average sediment load ($\bar{Y}_{(k)t}$) in kilograms passing over the k^{th} plate (of width W_p). Here, 'average' refers to the mean of a Monte Carlo simulation, for which confidence limits can be derived. An estimate of the integrated cross-sectional sediment load over time step t ($\bar{Y}_{(total)t}$) can be achieved either by assuming a constant sediment load per unit width over each plate's respective bed segment and summing the loads for each segment (summative method - Equation 1a), or through interpolation using a linear (Equation 1b) or non-linear (e.g. cubic spline) method.

Summative method:

$$\overline{Y}_{(\text{total})t} = \frac{W_b}{(\text{N} \times W_p)} \sum_{k=1}^{\text{N}} \overline{Y}_{(k)t} \quad \text{(kg)} \tag{1a}$$

Linear interpolation:

$$\overline{Y}_{(\text{total})t} = \frac{W_b}{(\text{N} \times W_p)} \sum_{k=1}^{\text{N}} \left[\overline{Y}_{(k)t} - \frac{\left(\overline{Y}_{(1)t} + \overline{Y}_{(\text{N})t}\right)}{4} \right] \quad \text{(kg)} \tag{1b}$$

Assuming a linear interpolation will only slightly reduce the load from the summative method, a function of reducing sediment transport to zero at the margins, but is recommended if only one or two plates are installed. With three or more plates the choice of lateral integration function becomes less important and the summative method can be adopted in most cases with reasonable

confidence in estimates. If necessary, unequal spacing of impact plates across the bed can be accommodated in the model but with variants of Equations 1a and 1b. The use of multiple plates, therefore, overcomes the tendency highlighted by Ferguson (2003) for width-averaging in one-dimensional approaches to underestimate the true bedload transport rate for cases where hydraulic conditions vary over a cross-section; such cross-sectional variability in transport is shown clearly by Downs et al. (2016). $\bar{Y}_{(total)t}$ can then be converted into unit rate of bedload transport (kg s^{-1} m^{-1}), also within confidence intervals, by dividing by the time step interval and bed width, offering the prospect of evaluating the relationship between discharge and bedload transport rate that is frequently derived in fluvial studies.

The above procedure is iterated through the monitoring period to complete R time steps and derive total cross-sectional sediment yield for that timeframe ($\bar{Y}_{(total)}$) within confidence limits. If monitoring for a period of months or years (with the objective of capturing the full, or near-full, spectrum of sediment transporting events), a longer-term sediment yield or, potentially, the average annual sediment yield can then be derived and the distribution of sediment load with discharge class explored (i.e. effective discharge analysis).

2.2 Converting bedload impacts to bedload mass in transit

2.2.1 Characterizing sediment size and shape (Stage 1)

Analysis is initiated by deriving representative particle size and shape distributions from samples of bed material retrieved from locations in close proximity to the impact plates (Figure 2). Sediment size is equated to the intermediate (b-axis) diameter of particles. Both surface and bulk samples (volumetric subsurface) are required as the surface sediments control the critical shear stress required to disturb the bed and initiate bedload motion (Buffington and Montgomery, 1997), while material in transit is generally much finer than the surface and closer in size distribution to the bed substrate (Lisle, 1995). Composite size distributions from several samples are advised to accommodate the spatial variability of material in the channel bed and to achieve a reasonably large sample volume. Surface samples can be obtained in the field by using the standard grid-by-number method (Wolman, 1954, and see Bunte and Abt, 2001), while bulk samples can be sieved in the laboratory, acknowledging that coarse-grained beds require substantial sample sizes of tens of kilograms or even several hundred kilograms depending on the coarseness of the bed (Bunte and Abt, 2001; Church et al., 1987; Ferguson and Paola 1996; Mosely and Tindale, 1985). For surface material, a sample comprising 100 particles is suggested to yield an accurate median particle size whereas a

sample of 400 or more is required to accurately portray the shape and extremes of the distribution, and is thus important here (Rice and Church, 1996).

In the model, frequency distributions are converted to phi-scale (ϕ, = $-\log_2(d)$, where ϕ is the negative of the logarithm of size to the base 2) classes to correct for the positive skew inherent to most sediment size distributions, and interpolated using a spline function to produce a smooth, monotonic cumulative distribution curve (Fritsch and Carlson, 1980 - monotone cubic Hermite method). Separate splines for composite surface and bulk samples are developed at this stage, with the average of the surface material median particle sizes (d_{50}) extracted to use as the reference size in the equation of incipient bedload motion (Equation 4 in Stage 4, below).

Estimates of particle volume (Stage 4) are also influenced by particle shape. As an optional (but highly recommended) step, sediment shape is analysed from measurements of a-, b- and c-axis diameters (d_a, d_b and d_c, respectively) of individual bedload particles. The model stores this dataset as 100 frequency percentiles of the ratios d_b/d_a and d_b/d_c (following the shape classification scheme of Zingg, 1935). In the absence of sediment shape data, the model defaults to assuming all particles are spherical, although recognizing this will be a source of considerable bias in most cases.

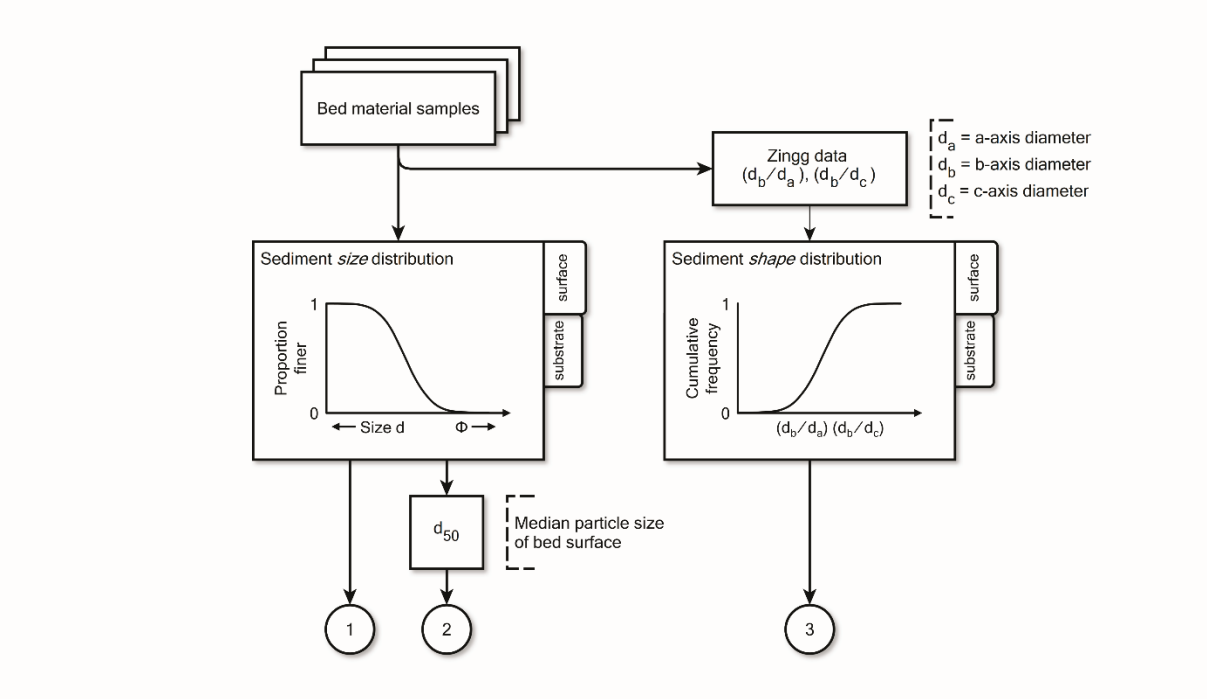

Fig. 2. Model Stage 1: Bed material characterization. Bed material particle size and shape distributions and median size of bed surface sediment are derived from composite bulk and surface samples. N.B. the connectors 1, 2 and 3 are subsequent inputs to Stage 4 (Fig. 5).

2.2.2 Estimating local water depth (Stage 2)

A representative cross-section is required, ideally surveyed at the site of the impact plates before their installation. In addition, a record of water surface elevation is needed to estimate the water depth over each plate for each instantaneous discharge (Figure 3). Depth here is used to estimate an average bed shear stress that drives the (theoretical) rate of sediment transport over and close to the impact plate and thus refers to a mean depth (D_m) within a 'shear stress panel' (SSP) centred on the plate. While hydraulic radius is conventionally used to estimate mean boundary shear stress for a cross-section, the SSP approach is preferred here with locally averaged depth restricting shear stress from being underestimated for plates sited close to the thalweg and overestimated for plates located in shallower water closer to the channel bank edge. This is particularly important where there is considerable variation in sediment transport rate across the section. For each plate, the default width of the shear stress panel is W_b/N - the bed width divided by the number of plates, although this can be set differently.

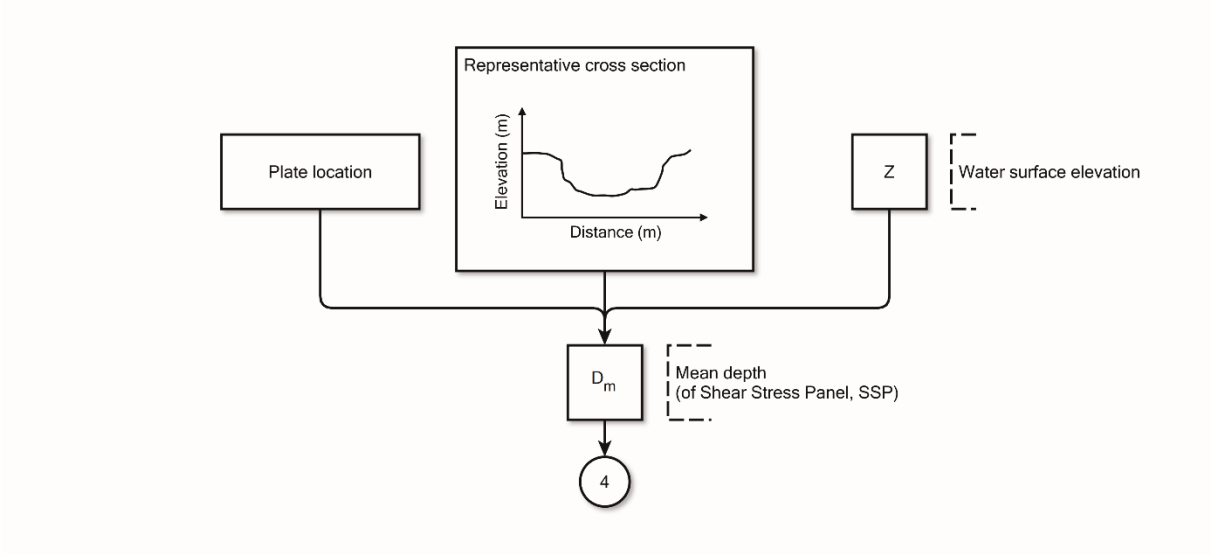

Fig. 3. Model Stage 2: Mean depth estimation over an impact plate, derived from the water surface elevation of each instantaneous discharge and the location of the plate within the cross-section. N.B. the connector 4 is a subsequent input to Stage 4 (Fig. 5).

2.2.3 Setup of model parameters (Stage 3)

A Monte Carlo routine attributes random combinations of sediment size (and therefore, mass) to each of the C recorded bedload impacts during time step t. This stage involves setting distributions for the parameters that constrain this process, using realistic bounds to the inputs rather than definitive values. The primary requirement is to set bounds to the minimum and maximum particle sizes that can be transported and detected as bedload by a given flow. This requires variables for the minimum particle size detectable by the impact plate (d_{min}), the Shields parameter (dimensionless

shear stress, a) and associated hiding factor (b), specific gravity (G), and the water surface slope (S) as a surrogate for the energy gradient (Figure 4, and details below). During each model iteration, values for each variable are selected at random from an assumed normal distribution, specifying an upper and lower value for each parameter associated with the central 95% of the measured distribution (or 1.96 * 2 standard deviations). These bounds are used to estimate the mean and standard deviation and thus the shape of the cumulative probability density function from which the Monte Carlo simulation selects the values for each iteration corresponding to randomly chosen probabilities. This is a conventional method for setting up the Monte Carlo process and has been applied, for example, by Pitlick et al. (2009) to evaluate uncertainty in modelled sediment transport estimates.

The minimum particle size detectable by the impact plate (d_{min}) varies according to the impact plate design and so requires laboratory and experimental calibration. The current design of 'Benson-type' plates used here has a d_{min} of c. 10±2 mm, established through limited flume testing (Downs et al., 2016). Impacts are recorded whenever a threshold voltage of 20 mV is exceeded and a detection frequency of approximately 5-7 Hz is used to restrict potential issues with over-counting rolling particles (see footnote[1]).

The Shields parameter, hiding coefficient, specific gravity and slope relate to the critical shear stress for mobilizing sediment of a particular maximum size, according to the following relationships. Equation 2 is a simplified version of the original formula of Shields (1936) and Equation 3 is the conventional expression for accounting for protrusion and hiding effects in mixed beds, as proposed by Andrews (1983):

$$a_x = \frac{D_m S}{(G-1)d_x} \tag{2}$$

[1] All bedload measurement techniques are subject to issues of potential bias and impact sensors and geophones are no exception, with potential issues of consistency related to grain-size dependency and transport-style effects that will vary with the design of the sensor. For example, experiments with the Swiss-plate geophone indicate signal response is partially dependent on particle size (e.g. Rickenmann et al., 2012, 2014; Rickenmann and Fritschi, 2010; Rickenmann and McArdell, 2007; Wyss et al., 2016a, 2016b, 2016c) and other experiments have suggested that rolling particles may record more impacts than sliding or saltating particles (Turowski and Rickenmann, 2009). Here, over-counting is limited by using a small plate to physically-restrict multiple contacts and setting the detection frequency to suppress very closely timed impulses (the sensor is set to approximately 5-7 Hz). Limited flume testing of the Benson-type plates used (R. Carrillo/P. Downs, unpublished data; I. Benson, unpublished data) suggests variable recording efficiencies but no consistent bias for grain size is yet proven to date. One advantage of using the BLIP model, wherein grain size characteristics are estimated probabilistically, is that the model could readily be altered in a future revision to offset a proven bias using a correction factor for grain size.

$$\frac{a_x}{a} = \left(\frac{d_x}{d_{50}}\right)^{-b} \quad (3)$$

Here, 'a' refers to a reference Shields Parameter, related to a reference grain size (considered here to be the median size of surface material, d_{50}, as specified by Buffington and Montgomery, 1997), 'a_x' is the Shields parameter related to individual particle size d_x and 'b' is the hiding factor. In Equation 2, mean depth, D_m, refers to depth for the SSP (see Stage 2).

Equation 2, alone, assumes for a given Shields parameter that shear stress (expressed by D_mS) is linearly proportional to sediment size (i.e. entrainment is purely size-selective). With the addition of the hiding coefficient in Equation 3, it is possible to model a range of conditions from pure size-selectivity (b=0) to equal mobility of all grain sizes (b=1), whereby protrusion of coarser than average sizes and hiding of finer than average sizes cancel out their size selectivity.

Substituting Equation 2 into 3 and rearranging to make d_x the subject yields an expression for the largest particle size that can be mobilized at this condition (renaming d_x as d_{max}), for b<1:

$$d_{max} = \left[\frac{D_m S}{a(G-1)d_{50}^b}\right]^{\left(\frac{1}{1-b}\right)} \quad (4)$$

When b=0 in Equation 4, the expression reduces to a rearranged form of Equation 2. Critically, in the model d_{max} is capped by the largest particle size obtained from the field bulk samples. Entrainment of particles of diameters up to d_{max} requires specification of the Shields parameter (a) and hiding factor (b) in Equation 4 (see supplementary material: selection of Shields parameter and hiding factor).

In setting up the model, water surface slope can either be set to adjust with water surface elevation when stage is monitored with two or more pressure transducers (see insert in Figure 4), or held constant (recognizing that in many applications there may be difficulties in measuring slope over time). Upper and lower slope limits are entered that are assumed to correspond to the 95% confidence level.

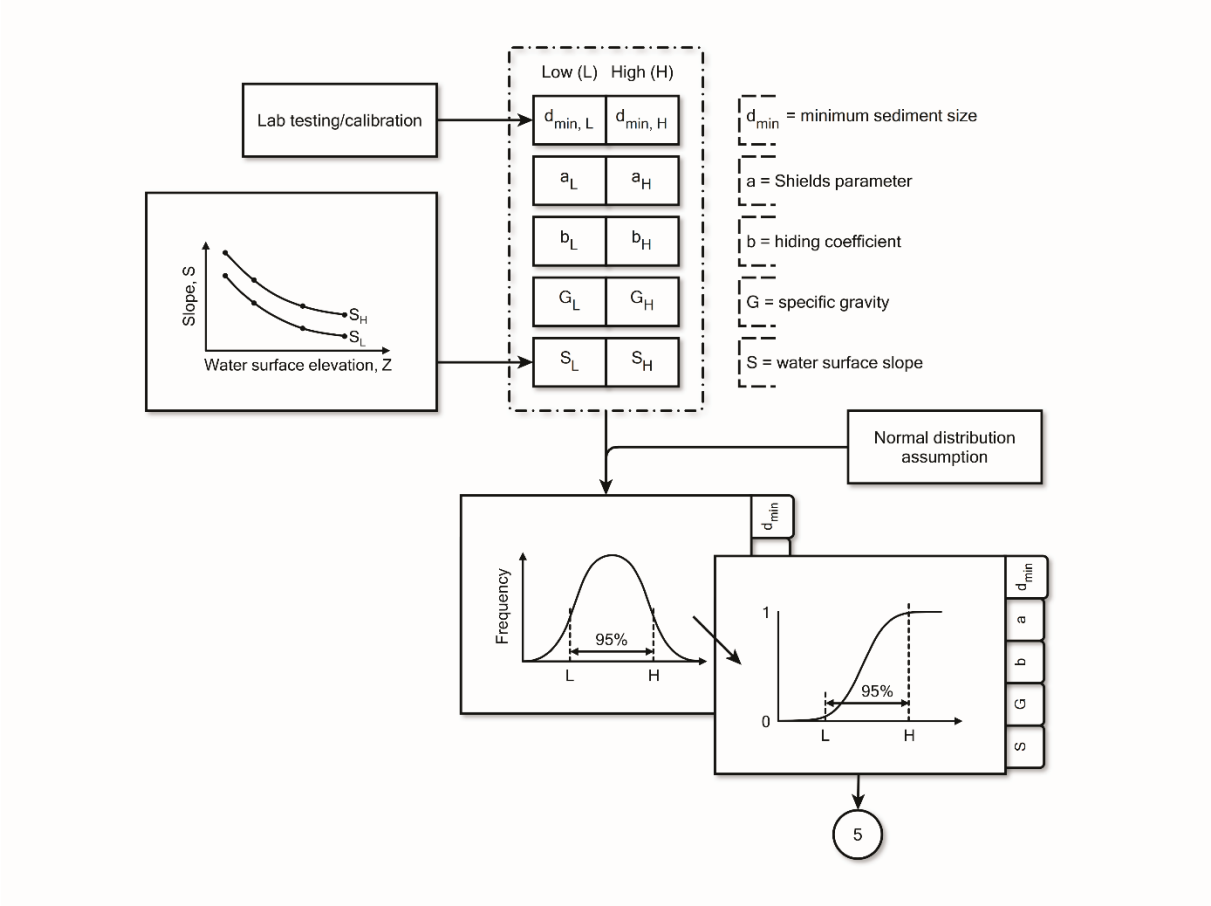

Fig. 4. Model Stage 3: Uncertainty-bounded parameterization of minimum (detectable) sediment size, Shields parameter, hiding factor, specific gravity and water surface slope. These bounds are used to estimate the corresponding cumulative probability density functions used in the Monte Carlo simulation. N.B. the connector 5 is the subsequent input of the cumulative distributions to Stage 4 (Fig. 5).

2.2.4 Monte Carlo simulation (Stage 4)

Accounting for uncertainty and investigation of sensitivity is important in developing any model (Jakeman et al., 2006) and Monte Carlo methods are the simplest means of conducting such analyses (Uusitalo et al., 2015) and highly flexible to any model code (Refsgaard et al., 2007). Here, uncertainty is integral to the modelling process and not considered as an 'end-of-pipeline' audit (Refsgaard et al., 2007). Monte Carlo analysis is well-suited for framing the variability of sediment transport potential in relation to discharge and has previously been applied in fluvial studies (e.g. Han et al., 2015; Little and Biedenharn, 2014; Rustomji and Wilkinson, 2008; Warrick, 2015).

In this main computational stage of the model process, sediment load is probabilistically estimated for each recorded discharge-impact count pairing (i.e. at each time interval of data) (Figure 5). The number of model iterations for each time interval can be fixed by the user, although 1000 is recommended. For each iteration (i) a random probability is generated and corresponding input

parameters ($d_{min,i}$, a_i, b_i, G_i, S_i) are derived from their respective (bounded) cumulative normal distributions. Investigators have the option of fixing any of these parameters by equating their low and high bounding values in Figure 4, for example if specific gravity is known to be constant for a particular physiographic region.

Initially, with $d_{min,i}$ constant, and $d_{max,i}$ calculated from Equation 4, the bounds of the recorded sediment size distribution (from the composite bulk sample) are reset with probabilities (proportion finer) of 0 and 1 corresponding to the minimum and maximum values, respectively (inset in Figure 5). As such, the revised distribution includes only those particle sizes that can be sensed by the impact plate at the individual time step and discharge, within acceptable bounds of uncertainty. At each iteration, multiple inner computational loops are performed to interpolate C random particle sizes from the cumulative frequency distribution of sediments (where C is the number of recorded bedload impacts at the current time step).

For the jth particle size (of C) selected, d_j, the mass Y_j is calculated. This is achieved by assuming either a random cuboid particle shape (sampling at random from the distributions of d_b/d_a and d_b/d_c to estimate d_a and d_c, assuming the generated d_j corresponds to the b-axis diameter, d_b, in the above ratios), or alternatively a sphere. In the former case, the simulated volume is likely to slightly overestimate the true volume of a particle (as corners are somewhat rounded) but is probably more accurate than assuming a sphere, particularly for more disc-shaped (oblate) or rod-shaped (elongated/prolate) clasts. The summed logarithmic mass of the C particles is then stored in an array and Stage 4 is repeated for the next (i+1) iteration. Upon completion of the i-loop (e.g. 1000 iterations), the geometric average mass from the array is computed, together with confidence limits at a chosen significance level (default 95%). Two measures of uncertainty are employed: i) confidence limits on the mean (mean response); ii) percentile confidence limits corresponding to the range of mass between the tails of the distribution (single response, or 'prediction' limits), i.e. (100-α)/2% to (100+α)/2% at the α% confidence level. The percentile confidence limits are perhaps the better representation of the variability and inherently non-deterministic nature of bedload transport.

On completion of Stages 1 to 4, results are integrated from the series of plates across the section (Figure 1) to derive the total cross-sectional load for the current time step (with confidence limits) before proceeding to the next time step, and corresponding discharge and stage. The model continues through the monitoring dataset for all recorded impact counts until a total cross-sectional yield over time ($\bar{Y}_{(total)}$) is obtained. Thus, a probabilistic rate of bedload transport is obtained from

knowledge of impact counts, the bed material distribution and parameters of the flow and cross-sectional geometry.

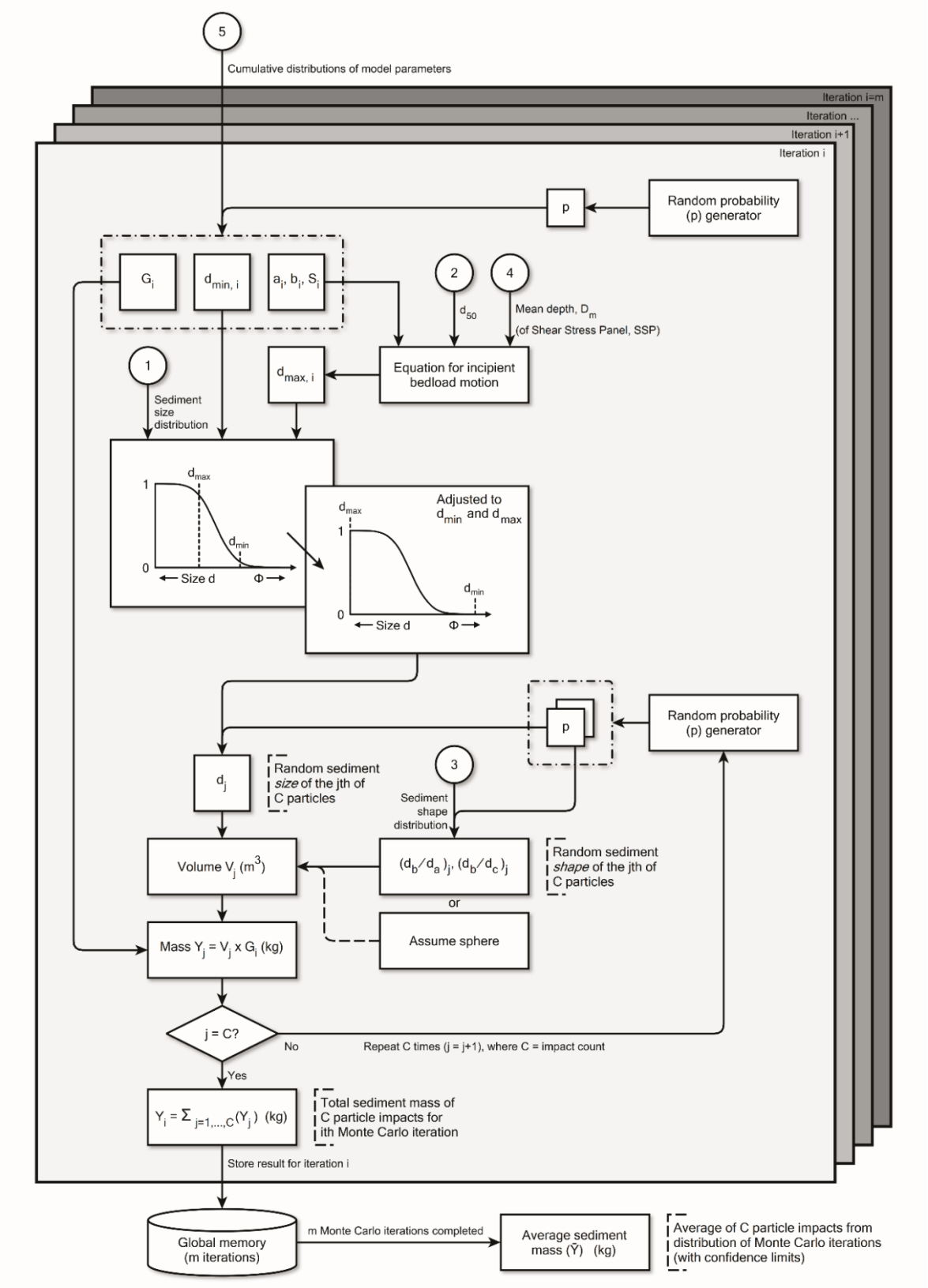

Fig. 5. Model Stage 4: Bedload mass calculation by Monte Carlo analysis. The input bedload size distribution is constrained to include only those particle sizes that can be detected and transported over the current time step, at the corresponding

discharge and stage. The mass of each particle detected over the time step is estimated randomly from the size distribution and the total sediment mass (with confidence limits) derived iteratively through the Monte Carlo process. N.B. the connectors 1-5 are inputs from Stages 1-3 (Figs. 2-4).

3. Application

The approach was applied to seismic impact plate data monitored near the mouth of the River Avon, a flashy, gravel-bed river in South West England (drainage area 110 km^2). The study reach is characterized by an abundant supply of bed sediment fed from local sources during moderate flows up to barfull but with notable sediment supply limitations during high in-bank events (Downs et al., 2016). The bed material has a composite median (d_{50}) bulk grain size of 15 mm, surface d_{50} of 34 mm, and water surface slopes vary typically from 0.0030 in moderate flow to 0.0025 during high overbank flow. Fifteen-minute discharge data are recorded at a gauging station approximately 1 km upstream of the monitoring site. Impact counts were recorded for 150 x 130 x 6 mm plates mounted on a 400 x 400 mm paving slab at 2.5-minute intervals. The data, aggregated to 5-minute intervals from May 2012 to April 2013, coincided with the wettest period on (gauged) record including twenty overbank (>32 m^3s^{-1}) events and the maximum gauged instantaneous peak flow (124 m^3s^{-1}). The primary impact plate, IP1, was installed in the mid-channel thalweg of a straight, 12.0 m active bed width section of an otherwise geometrically complex alluvial meandering reach. Two further plates were installed in December 2012 to provide an array of three equidistant devices. Data from IP1 indicated a strong general correspondence between high flow events and high impact counts but with considerable scatter between 5-minute interval discharges and impacts (R^2 = 0.38) which was only slightly improved (R^2 = 0.49) when using an array of three impact plates (IP1 – IP3). The variability was partly attributed to significant and consistent within-event hysteresis. Aggregating event-total IP1 impacts against event-volumetric discharge (events averaged 32 hours in duration) increased explanation (R^2 = 0.74) as intra-event and stochastic bedload factors were subsumed. Further details on the catchment, reach and experiment are provided by Downs et al. (2016).

4. Results

4.1 Calibration

In predicting the largest grain size in motion (Equation 4) at any individual flow it is important to calibrate the method to a rational Shields parameter (a) and sediment hiding factor (b). In this regard, the monitoring data provide two critical 'known' components (see Downs et al., 2016). First, the minimum particle size capable of being recorded by the plate is c. 10±2 mm. On the River Avon

this occurs at approximately 4 m^3s^{-1} (i.e. threshold discharge of recorded impacts). Second, the majority of recorded transport occurs within a flow range of approximately 8-20 m^3s^{-1}.

The sensitivity of Equation 4 in the model to variations in parameters 'a' and 'b' is illustrated in Figure 6. By setting 'a' to 0.03 (the midrange value between 0.025 and 0.035 of Mueller et al., 2005), the resulting 'b' corresponding to a maximum entrained particle size of 10 mm (the threshold of bedload motion at 4 m^3s^{-1}) is approximately 0.6 (Figure 6b), invoking the midrange hiding factor suggested by Ferguson (2005).

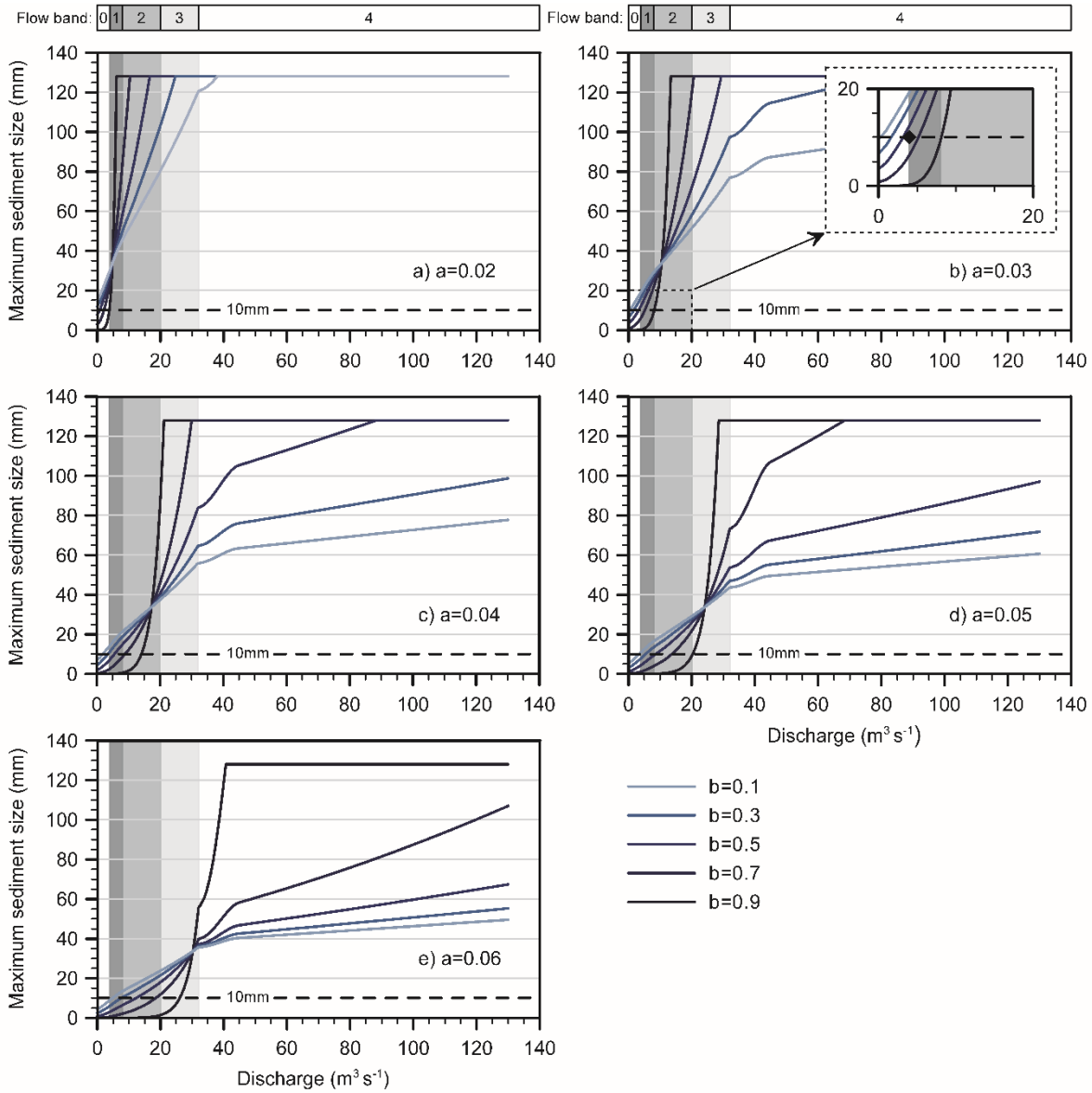

Fig. 6. Calibration of the method to Shields parameter (a=0.02 to 0.06) and sediment hiding factor (b=0.1 to 0.9). The insert in (b) shows for the maximum entrained particle size of 10 mm the hiding factor is approximately 0.6 when the Shields parameter is set at 0.03. Flow bands illustrate important thresholds to characterize bedload transport activity (based on

Downs et al., 2016) and are repeated through the sequence of Figs. 6 to 12. Band 0 (<4 m^3s^{-1}) = no recorded bedload impacts. Band 1 (4-8 m^3s^{-1}) = threshold of recorded impacts to point of rapidly increasing activity. Band 2 (8-20 m^3s^{-1}) = peak rates and majority of recorded bedload activity, where 20 m^3s^{-1} corresponds to the 'barfull' stage. Band 3 (20-32 m^3s^{-1}) = significantly reduced rates of recorded bedload where 32 m^3s^{-1} corresponds to the 'bankfull' stage. Band 4 (>32 m^3s^{-1}) = progressive increase in recorded rates with larger overbank flows.

These settings also predict significant entrainment in the 8-20 m^3s^{-1} range, known to account for most of the recorded sediment impacts. Applying much higher Shields parameter values (e.g. 0.05-0.06) requires a very low hiding factor indicative of conditions close to full selective entrainment in order to achieve 10 mm particle entrainment at 4 m^3s^{-1} (Figure 6d, e). Such parameters contrast markedly with the armouring characteristic of observed field conditions and also do not predict entrainment of the coarsest fraction of the substrate material. At the other extreme, conditions indicative of (near) equal mobility (low a, high b) are incapable of predicting accurately the threshold of particle recording (Figure 6a) and imply full mobility of the bed (horizontal line capping maximum size) much earlier than indicated by the impact counts (see discussion by Downs et al., 2016). For the River Avon, at least, field and laboratory data suggest that the best calibration parameters correspond to the mid-ranges suggested by Mueller et al. (2005) and Ferguson (2005).

4.2 Predicted bedload rates

Following initial calibration, multiple model runs explored the bedload dynamics of the lower River Avon. Various data ranges were assumed to correspond to 95% confidence bands based on field data or values reported in the literature. Thus, the Shields parameter 'a' was varied between 0.025 and 0.035 (after Mueller et al., 2005), the hiding factor 'b' between 0.5 and 0.7 (after Ferguson, 2005) and specific gravity between 2.55 and 2.75 (field samples). Water surface slopes were assigned values ranging from 0.0030 at 4 m^3s^{-1} to 0.0230 at 32 m^3s^{-1} (bankfull stage) and 0.0250 thereafter, all ±0.0003 based on field data from pressure transducers.

The primary impact plate (IP1), positioned centrally on the flow thalweg, recorded 27,850 'non-zero' intervals (i.e. five-minute intervals with at least one impact) from a total of nearly 92,300 intervals, implying bedload transport in approximately 30% of all five-minute intervals recorded in this wettest year of gauging records. In total there were approximately one million impacts, thus (with 1000 Monte Carlo iterations per impact) requiring approximately one billion model iterations to establish a confidence limit-bounded time-series of average impact mass. Processing time took approximately 2 hours 45 minutes on a PC with Intel quad-core i5 processor and 8 GB RAM. When performing model runs for different impact plates, and when investigating the effect of varying input parameters,

overall computation time was reduced by employing several computers. The basic time-series output of average mass from the model (Figure 7) indicates unit rates up to a maximum of nearly 0.7 kg s^{-1} m^{-1} passing across the plate/slab combination. Loads vary in general by at least two orders of magnitude explained in part by the geometric scale of the particle size distribution but also indicating the substantial role of supply limitations (see Section 5.1). Truncation of maximum transport rates can result from saturation of the impact plate data loggers (139 of 92,284 5-minute periods) and/or periods when flow exceeded that required to transport the coarsest bed sediment.

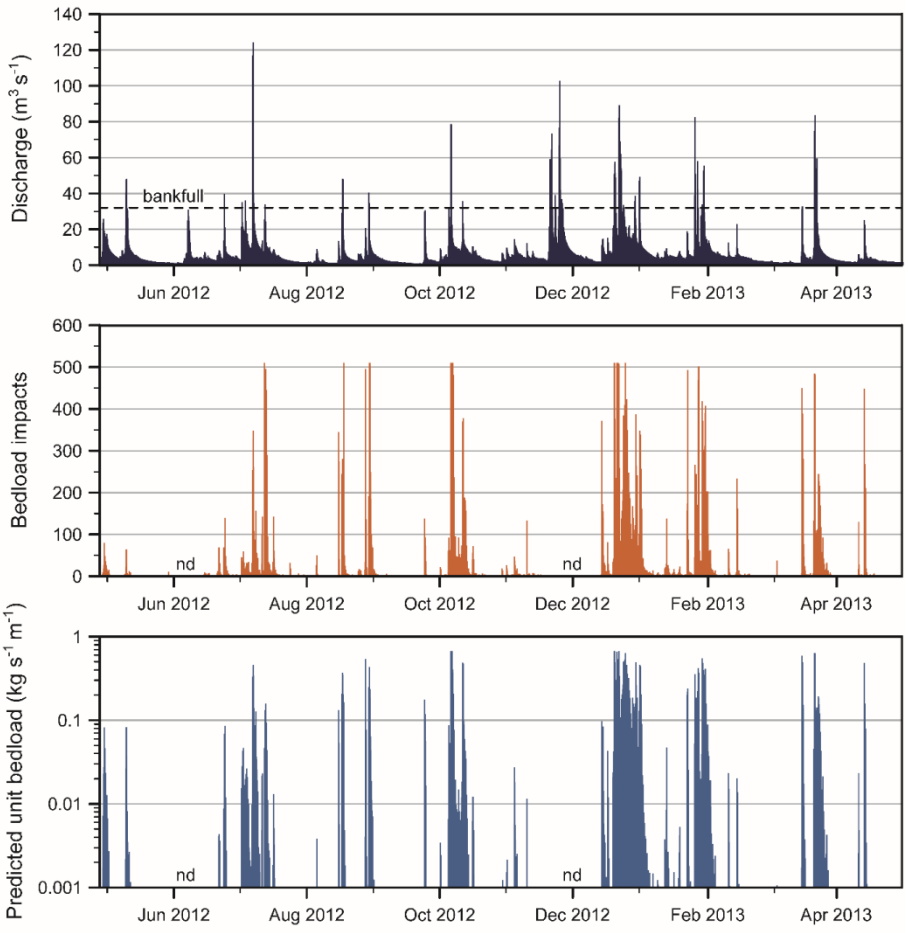

Fig. 7. Time-series of gauged discharge, impacts recorded by Impact Plate 1 and corresponding predicted (average) unit bedload rates from late April 2012 to early May 2013. Impacts are aggregated to 5-minute intervals with a maximum of 510 counts in each period. Data gaps (nd) occur where safe retrieval of the plates was impossible. The discharge record is interpolated from the series of 15-minute gauged flows.

The distributions of impacts and predicted unit rate of bed load at 5-minute intervals are illustrated in Figure 8 for the 12 month period of monitoring at plate IP1. Progressive entrainment of coarse bed material occurs after the 4 $m^3 s^{-1}$ minimum threshold for instrument detection (Figure 8a) until

approximately 8 m^3s^{-1}. Subsequently, impacts rapidly peak (including occasional instrument saturation) until decreasing again above about 20 m^3s^{-1}, which is morphologically the level of barfull discharge. The average number of impacts then decreases until the morphological bankfull discharge of 32 m^3s^{-1}, beyond which impacts progressively increase with the magnitude of overbank discharge. The physical explanation for these dynamics appears to relate strongly to significant within-event hysteresis: analysis of 48 individual events (Downs et al., 2016) consistently demonstrated bedload spikes occurring during both the rising and falling limb of the hydrograph. Such hysteresis is assumed to represent supply variations related to break-up of the armour layer (rising limb) and bank failures and flood-routing of non-local sediment sources (falling limb). Anticlockwise hysteresis is dominant, particularly for the 20 overbank flow events, such that the peak in impacts, most clearly demonstrated by the locally-weighted 95^{th} percentile curve in Figure 8a, corresponds largely to bedload transported in flows decreasing from 20 to 8 m^3s^{-1}, reflecting the complexity of local sediment supply when monitoring sediment discharge at 5-minute intervals (Downs et al., 2016).

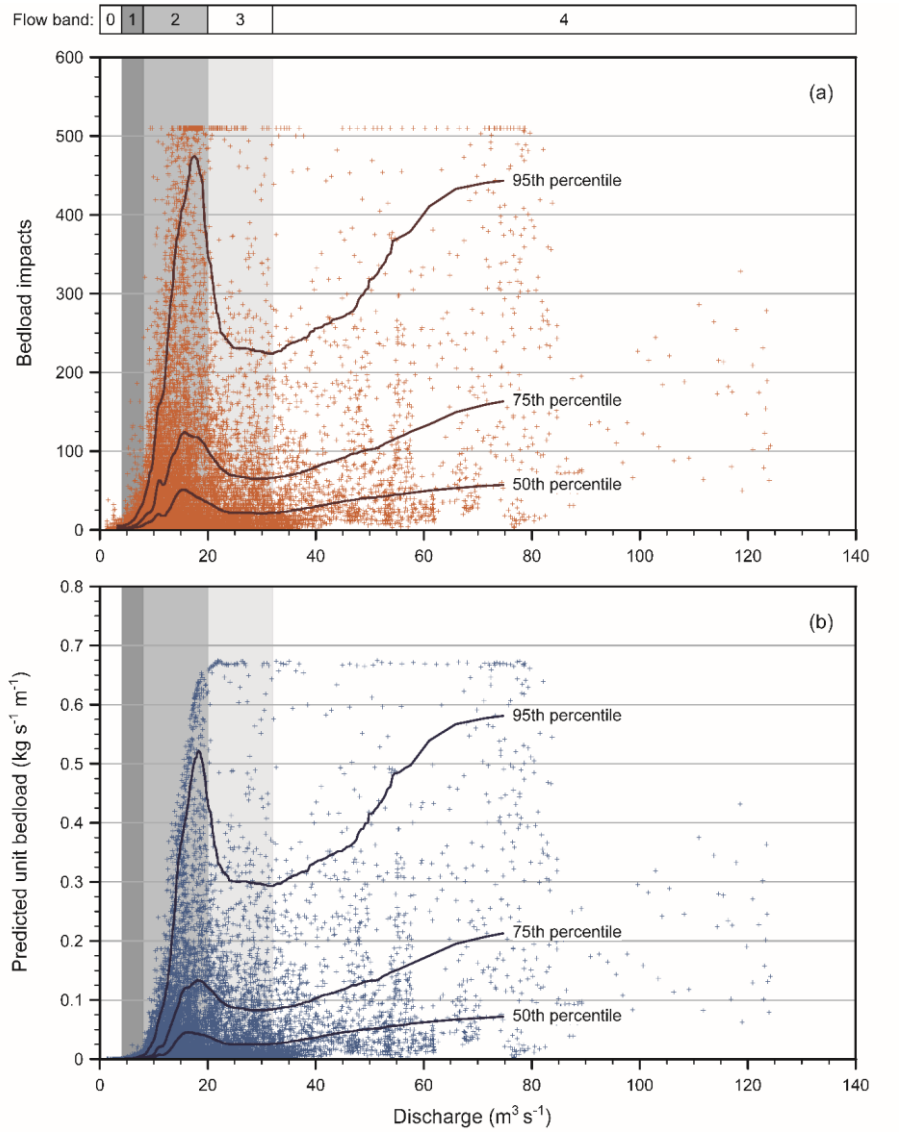

Fig. 8. Instantaneous discharge versus 5-minute impact count totals for Impact Plate 1 (a) and corresponding predicted (average) unit bedload rates (b) for 27,850 non-zero records during the 12 month study period (late April 2012 to early May 2013). Data saturation occurs in 139 (0.5%) of the total non-zero impact periods. Indicative 'weighted' percentiles highlight the variability with discharge (based on a moving window through 10% of the dataset and a Gaussian kernel smoothing algorithm to weight points according to proximity to the centre of the window).

A similar pattern is indicated in Figure 8b when impacts are processed through the model to produce unit bedload rates across plate IP1. Relative to the impacts in Figure 8a, appreciable sediment transport loads are offset towards slightly higher discharges, caused by multiplying the particle impacts by their volumetric mass. Also, there is a far clearer 'leading edge' to the predicted loads related to the monotonic increase in maximum transportable size with discharge and the averaging effect of the Monte Carlo simulation (Figure 8b). Despite the offset at low discharges, though, peak

rates of transport (most clearly depicted by the 95th percentile curve) occur at approximately the same discharge (18 m^3s^{-1}) as the peak rate of impacts.

Records from the three plate array for mid December 2012 to early May 2013 miss the peak instantaneous flow of record (7 July 2012; approximately 90-year recurrence interval) but do include the wettest daily average flow of record during late December 2012. The lateral variability in bedload transport (Figure 9) is evident in that at no point does saturation occur simultaneously in all three plates (which would cap impacts at 510 x 3 = 1530 impacts). Indeed, the resulting pattern of impacts generally reflects the combination of impacts at IP1 (thalweg) and IP3 (river right), with very few impacts occurring over plate IP2 (river left) (see Downs et al., 2016, their Figure 12). Also, a broader peak in impacts exists in Figure 9a than in Figure 8a because impacts at IP3 and IP1 are not coincident. Impacts at IP3 occur primarily on the falling limb of the hydrograph; field evidence suggests this reflects an increasingly diagonal flow path during flood recession that transports a large volume of finer gravels over IP3. Changes to the pattern of impacts consequently alters the distribution of modelled cross-sectional bedload rates (Figure 9b), with a few overbank unit peaks now between 0.25 kg s^{-1} m^{-1} and 0.35 kg s^{-1} m^{-1}. Comparing Figures 8b and 9b indicates that the out-of-phase impacts at IP1 and IP3 result in peak cross-sectional transport rates of approximately 35 per cent that of IP1 alone (i.e. based on comparison of the locally-weighted 95th percentile curves), whereas the median transport rates shown by the 50th percentile curves are similar at approximately 0.05 kg s^{-1} m^{-1} (acknowledging here that Figure 9b relates to a shorter monitoring period). The discharges at which peak transport rates occur do not change.

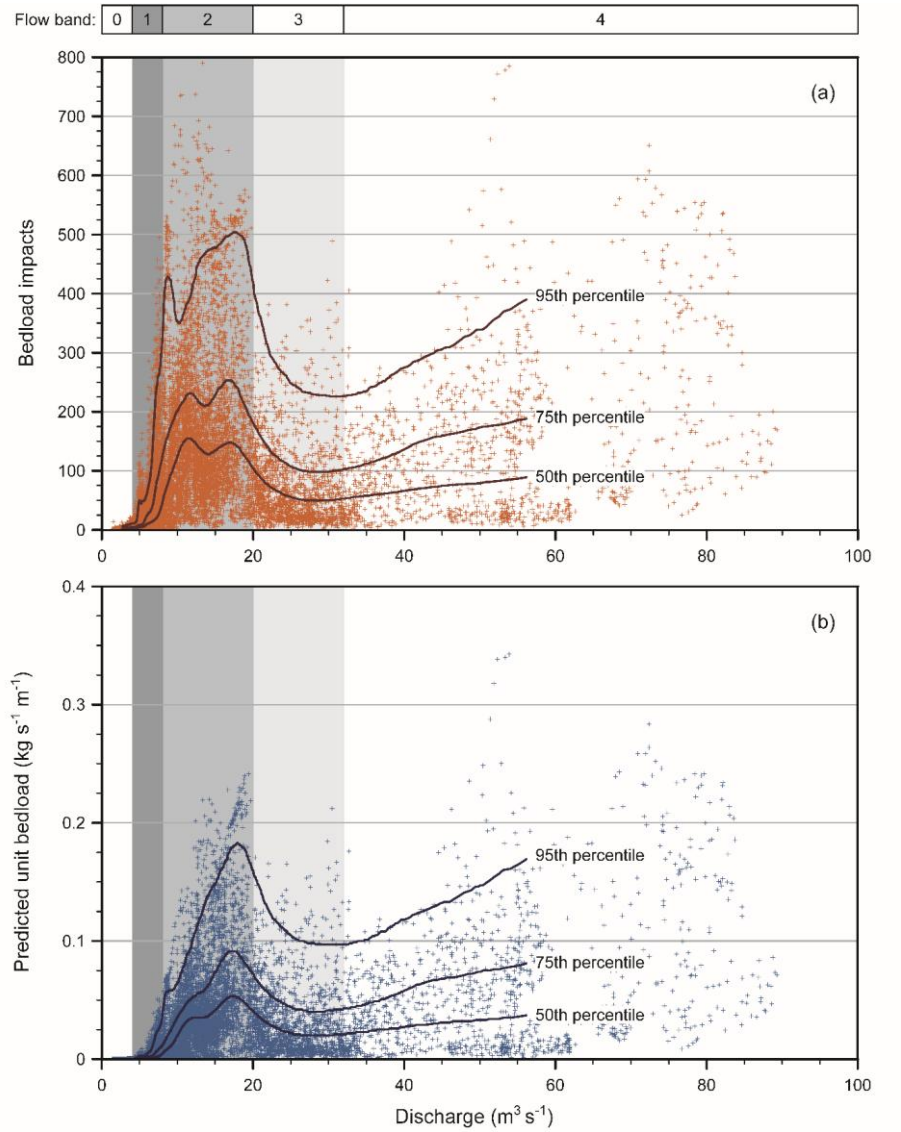

Fig. 9. Instantaneous discharge versus 5-minute impact count totals for Impact Plates 1 to 3 combined (a) and corresponding predicted (average) unit bedload rates (b) for the cross-section. Results are for 13,181 non-zero records during the 4.5 month period (mid December 2012 to early May 2013) in which all three plates were installed. Indicative weighted percentiles highlight the variability with discharge.

5. Discussion

This approach to bedload rate estimation constitutes a probabilistic estimate of transport derived directly from impact counts. It is semi-empirical and data-driven, an alternative to traditional approaches to bedload estimation that involve either direct measurements, producing a fully river-constrained estimate of bedload but requiring a lengthy calibration process, or those resulting from bedload transport formulae that can be achieved very rapidly but have very limited locational specificity. There are two particularly distinct attributes of this methodology. First, the approach is 'autogenically moderated' by incorporating the effect of near-instantaneous variations in sediment

supply derived from the high-resolution dataset obtained from impact plates (or other passive measurement approaches). Second, the model enables rate estimates to be sensitivity tested and statistically-bounded for uncertainty - a process that is inherently logical given the variable nature of bedload transport.

5.1 Supply-limited bedload estimation

We interpret the modelled transport rates not as 'potential' (see Gomez, 2006) but as veritable representations of a river's bedload transport. This claim stems from an assumption that the high-resolution input dataset faithfully represents the complex multiplicity of processes (the 'stochastic', ontological uncertainty considered by Refsgaard et al., 2007) that results in sediment transport over heterogeneous beds (and which will always defy deterministic sediment transport formulae). As such, the modelled bedload rates are autogenically moderated by impact counts that are effectively accommodating intra- and inter-event sediment supply variations. The model is thus intrinsically unlikely to overestimate sediment loads, a known area of concern for sediment transport functions in supply-limited conditions (Barry et al., 2004; Bathurst 2007; Bravo-Espinosa et al., 2003; Gomez, 2006; Recking, 2012; Vázquez-Tarrío and Menéndez-Duarte, 2015). As this moderation is internal to the model as a verification process, the model is potentially portable to other sites and does not require long periods of data 'training' to produce site specific estimates of bedload transport: a considerable advantage over methods that are constrained by calibration to measured loads. Indicatively, the peak unit transport rates for the cross-section lie comfortably within the range of values reported in the literature: a lower bound of 0.1-0.2 kg s^{-1} m^{-1} (e.g. Carling, 1989; Reid et al., 1985; Vázquez-Tarrío and Menéndez-Duarte, 2015) and a guideline upper bound of 1-3 kg s^{-1} m^{-1} (e.g. Bathurst, 2007; Habersack et al., 2008; López et al., 2014; Vericat and Batalla, 2010; Whitaker and Potts, 2007). Conceivably, the modelled values here may fall below the suggestive upper bound simply because the impact plates only detect particles greater than 10 mm.

The accuracy of the approach instead depends on instrument factors, choice of a representative cross-section and adequate characterization of the surface and bulk sediments, threshold of bedload motion and water surface slope. The accuracy in estimating cross-sectional sediment loads undoubtedly improves with number of plates deployed, enabling their measurements collectively to reflect the bedload transport dynamics. Further, the high-resolution dataset enables the effects of temporal variability in transport rates (over flow events and between years of data) to be examined, while arrays of impact plates within a project reach enable the spatio-temporal variation in bedload activity to be investigated (see Downs et al., 2016, for such exploration using bedload counts). In

realizing these value-added prospects, the modelling approach represents a credible alternative to commonly-utilized, time-invariant sediment transport equations (Recking et al., 2012) when addressing river management concerns.

5.2 Bounding transport rate uncertainties

Uncertainty analysis is employed here to facilitate investigation of sensitivity associated with the chosen entrainment parameters, the time-base of the rating relationship and bedload transport volume when integrated over longer time periods.

5.2.1 Entrainment

The model is clearly sensitive to the choice of appropriate ranges of the Shields parameter and hiding factor as constraints on the maximum size of sediment in transit. Thus, an important attribute of model evaluation is to investigate the influence of these parameters ('a' and 'b', respectively) on prediction of unit bedload transport rates. Three additional model runs were performed, estimating average transport rates from the central impact plate (IP1), but varying the 'a' and 'b' values, as illustrated in Figure 10 (here, Figure 10c reproduces the default condition in Figure 8b). These runs included the case of complete relaxation of the threshold of bedload motion (i.e. without imposing Equation 4) such that all sediment sizes were potentially available for transport (Figure 10a), a case of near equal mobility with 'b' ranging between 0.7 and 0.9 (Figure 10b) and the case of near selective entrainment with 'b' ranging between 0.1 and 0.3 (Figure 10d).

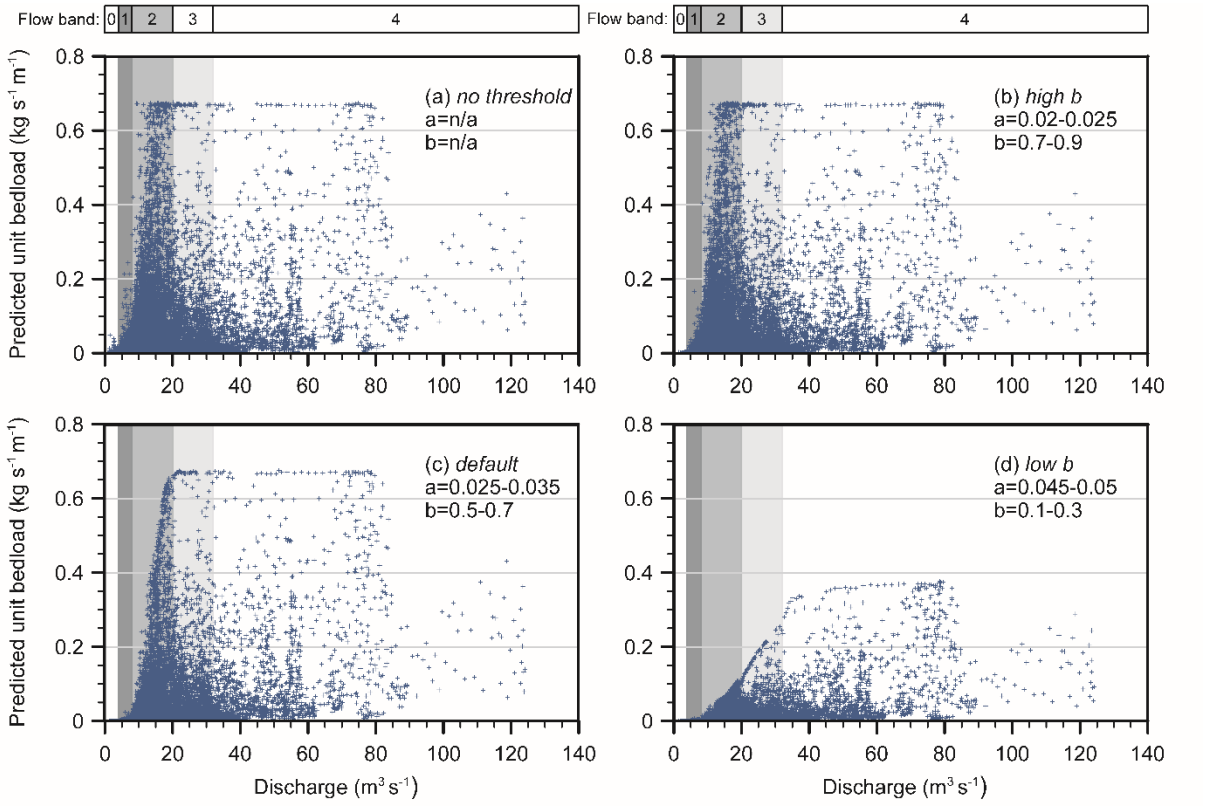

Fig. 10. Sensitivity analysis examining the influence of Shields parameter 'a' and hiding factor 'b' on the prediction of unit bedload transport rates. In (c) and (d) the Shields parameter was adjusted to maintain a minimum detection size of approximately 10 mm at the threshold of bedload motion of 4 m^3s^{-1} (see Fig. 6).

Relaxing the threshold for bedload motion (Figure 10a, b) results in the achievement of maximum transport rates at approximately 12-14 m^3s^{-1}. Here, the mobility of smaller gravels is limited due to the hiding effects and the protrusion of larger particles is elevating their transport potential at low flows. Maximum transport rates are thus achieved at some 4-6 m^3s^{-1} below those indicated by field data (Figure 8b, 10c), lending analytical support to observed partial bed armouring in delaying maximum rates of transport (see discussion in Downs et al., 2016), and indicating that using the Shields parameter at the lowest range of published values results in an unrealistic level of available sediment at flows only marginally above the threshold for entrainment (4 m^3s^{-1}, here). With progressive reductions in hiding/protrusion effects due to particle interactions on the bed (i.e. moving from Figure 10a to 10d) and an associated trend toward wholly size-selective transport, the leading edge of the point distribution is flattened, offsetting full particle mobility and maximum transport rates to higher discharges. Therefore, in Figure 10d, which illustrates the extreme case of selective entrainment based on size alone, the larger particles are not mobilized at all (the maximum size transported is 70 mm, compared with particles up to 128 mm in the bulk sample). This effect nearly halves the maximum transport rate and reduces average annual bedload yield over IP1 by 73

per cent compared with Figure 10c. In particular, there is a significant suppression of predicted transport activity at flows below bankfull discharge, a condition more akin to very stable armoured beds and much lower rates of sediment supply than experienced here during the remarkably wet study period.

5.2.2 Time-base

The modelling approach also allows the indirect generation of sediment rating relationships for detectable bedload using the high-resolution dataset to construct an autogenically moderated curve that reflects variable sediment supply conditions rather than the supply-unlimited potential inherent in sediment transport equations. It also allows an examination of the optimal time-base for rating relationships in striking a balance between high data resolution and reduced data scatter (Figure 11).

Ratings for plate IP1 (Figure 11a) reveal that with an increasing time-base and thus reduction in sample size, the rating curve exponent increases and the coefficient decreases (up to a slight reversal for the 24-hour time-base). Variance explained by the rating curves increases markedly from 5-minute to 1-hour intervals, with the R^2 plateauing at nearly 80% thereafter. Comparing the ratings between plate IP1 and the three plate cross-section (Figures 11a and b, respectively) suggests higher explained variance for the cross-section at the 5-minute time-base, but slightly lower explained variance for other periods (but note that Figure 11b relates to a shorter monitoring period). Conceivably, the plate array better captures the dynamic lateral variability of bedload transport at very short time periods but, at longer time periods, the out-of-phase impacts recorded between the different plates (see Downs et al., 2016) causes lower overall explanation.

Increasing the time-base for the full cross-sectional bedload (Figure 11b) shows marginal improvements in R^2 for rating curves capped at bankfull discharge (32 m^3s^{-1}) but little improvement is evident beyond the 1-hour time-base for rating curves capped at barfull discharge (20 m^3s^{-1}). Nonetheless, previous work by Downs et al. (2016) revealed an R^2 of 0.45 (with discharge capped at 20 m^3s^{-1}) based on impacts alone and thus the suite of unit transport rate exponents between 0.73 and 0.77 in Figure 11b appears to confirm an improvement in the predictive power of the rating relationship when bedload impacts are converted to average rates of unit bedload transport using the model.

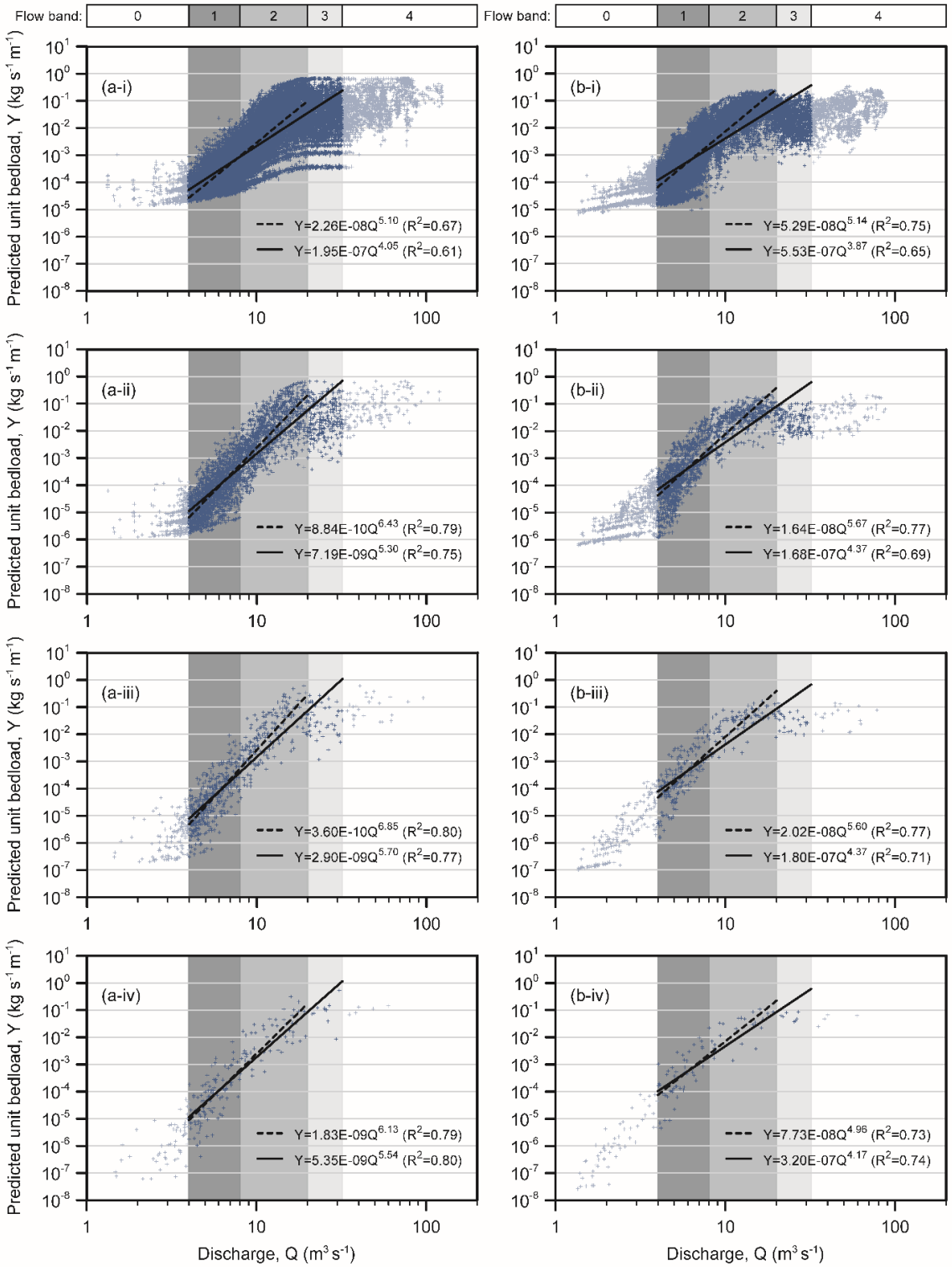

Fig. 11. Predicated (average) unit bedload rating relationships from 5-minute flow periods (i) compared to those derived by averaging discharges and aggregating impacts over 1-hour (ii), 6-hour (iii) and 24-hour (iv) periods, and for rating relationships constrained to the bankfull (32 m^3s^{-1} - solid line) and the barfull discharges (20 m^3s^{-1} - dashed line). The ratings for impact plate 1 (a) over the 12 month study period (late April 2012 to early May 2013) are set against those for the cross-section (b) over the 4.5 month period (mid December 2012 to early May 2013) with impact plates 1 to 3 installed.

Overall, the rating relationships capped at barfull discharge appear to be stronger than for those capped at bankfull discharge, attributed to the decline in peak bedload activity between 20 and 32 m^3s^{-1} (flow band 3 in Figures 8b and 9b). The rating exponents lie toward the upper range of 2-4 based on Helley-Smith sampling and at the lower range of 5-20 for rates derived from trap sampling (Bunte et al., 2014; Bunte and Abt, 2003). Using a large aperture sampler in a stream with many similarities to the Avon, the exponent range of 2.4-6.7 derived by Whitaker and Potts (2007) encompasses the values in Figure 11, giving further reassurances on average rating gradient. Very provisionally for the River Avon, the results may also suggest that rating curves averaged over a 6-hour time period provide the computationally most effective means of interpreting the coarse bedload flux for management purposes, while confirming that, scientifically, such averages conceal the significant variability inherent to sediment transport dynamics.

5.2.3 Transport volume

The Monte Carlo basis for the approach enables uncertainty-bounded 'average' bedload yields to be derived using a magnitude-frequency analysis (details in Downs et al., 2016). Figure 12a illustrates the distribution of bedload corresponding to particles detected by plate IP1 for each 1 m^3s^{-1} flow interval based on the full one year monitoring period (with default run criteria described above). A clearly defined effective discharge of 15-16 m^3s^{-1} is evident, which compares with a range of 13-15 m^3s^{-1} (and slightly less well defined peak) for the impact data alone (Downs et al., 2016). The offset to a slightly higher discharge is attributed to the conversion to volume and capping of maximum size of particles in transit within flow band 2 (8-20 m^3s^{-1}). Although Figure 12a reveals a clearly defined peak load, the 75% and 95% prediction limits reveal considerable uncertainty with the 15-16 m^3s^{-1} peak bedload increment varying between approximately 6.7 and 11.4 t at the 95% level. The cross-sectional sediment load over the 4.5 month winter monitoring period reveals a much broader bedload peak (Figure 12b) with discharges in the range 11-17 m^3s^{-1}, corresponding to the trend in recorded impacts (Figure 9a) and reflecting the lateral movement of the primary flow path over an individual hydrograph and resultant out-of-phase impacts between plates IP1 and IP3 (detailed by Downs et al., 2016). The total (>10 mm) cross-sectional load over the 4.5 month period averages 1455 t in this extremely wet period but is uncertainty-bounded to a range of 1273-1686 t (inter-quartile range) and 981-2218 t (95% limits). The bedload across flow band 2 (8-20 m^3s^{-1}) comprises almost two thirds (64%) of the total yield but with approximately ±10 per cent variation within the inter-quartile range. The availability of such uncertainty-bounded and autogenically-moderated estimates, when averaged over longer time periods, has potentially significant value in river

management and restoration planning, not least as the basis for estimating future changes in bedload fluxes.

As an essential component of the modelling protocol, sensitivity testing is encouraged to reveal how results might be affected by issues of data quality and to gain an understanding of potential sources of uncertainty. This can be demonstrated for the River Avon case study with two examples. First, by fixing slope to the average gradient of the bed (and thus unable to decrease with rising stage), it was found that while there was little impact to rates at discharges above barfull, cross-sectional bedload rates below this level were higher (with peak rates increased from 0.24 to 0.32 kg s^{-1} m^{-1}), the effective discharge was more clearly defined (but unchanged in value) and the average cross-sectional bedload yield over the 4.5 month monitoring period increased from 1455 to 1831 t. Second, by assuming all detected bedload particles are spherical, cross-sectional bedload rates were reduced for all discharges (reducing the peak rates below barfull from 0.24 to 0.16 kg s^{-1} m^{-1}), the effective discharge was less well defined (but unchanged in value) and the average cross-sectional bedload yield over the monitoring period decreased from 1455 to 1000 t; here, spherical particles (sized on the intermediate axis) are clearly underestimating the volume of more disc- and rod-shaped gravels typically found in the River Avon.

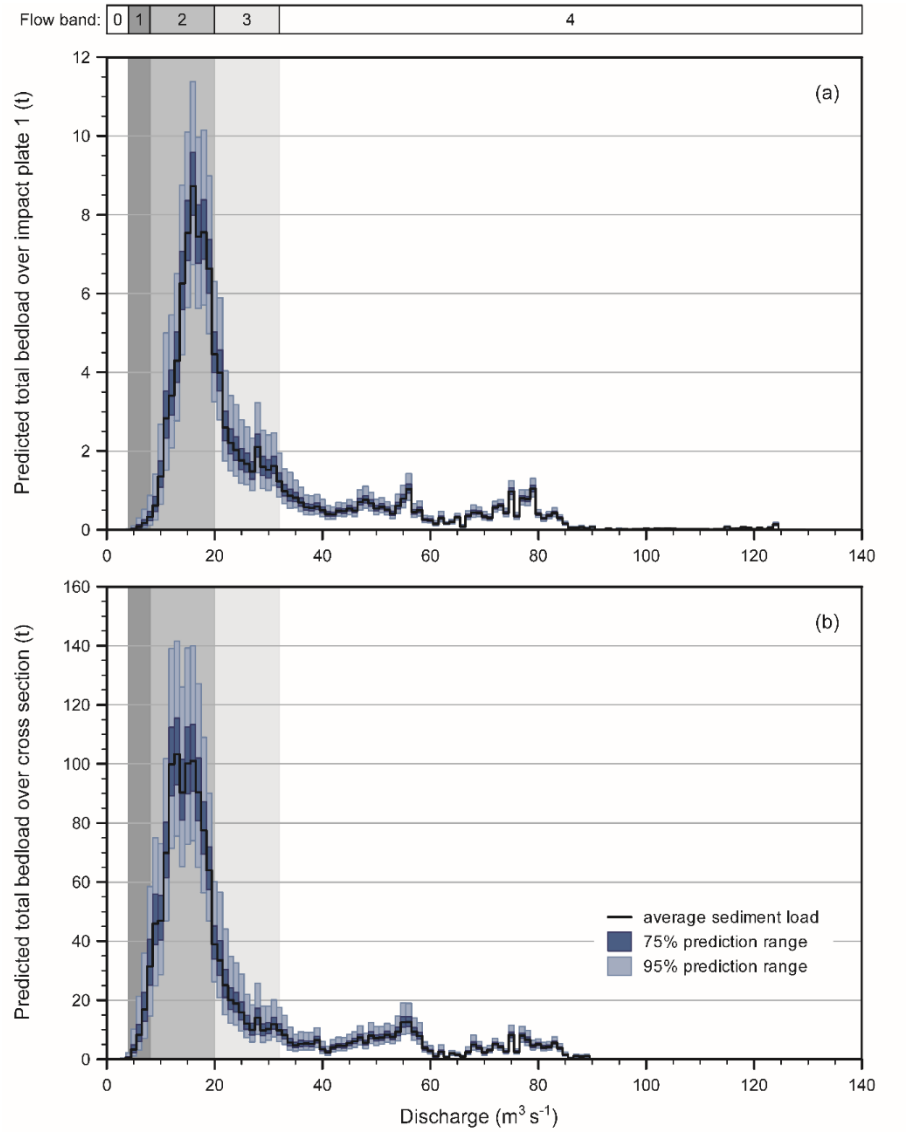

Fig. 12. Magnitude-frequency analysis of predicted total (>10 mm) bedload at 1 m^3s^{-1} increments for Impact Plate 1 (a) during the 12 month study period, illustrating an effective discharge equivalent measure for coarse bedload transport of 15-16 m^3s^{-1}, and for the cross-section (b) during the 4.5 month period with impact plates 1 to 3 installed, illustrating a broad bedload peak of 11-17 m^3s^{-1}.

6. Conclusion

Improvements to the prediction of bedload transport rates have been suggested to hinge on technological innovation (Ashmore and Rennie, 2012) and approaches that strike a balance between accuracy and practicability (Wilcock, 2001). Passive sensing devices offer considerable potential for generating high-resolution data over extended time periods to facilitate detailed insights into bedload dynamics not achievable with direct measurement methods or sediment transport formulae. However, despite a burgeoning suite of investigations exploring the accuracy and output dynamics of such sensors, converting the raw time-series of impacts into bedload transport rates and volumes

continues to remain a challenge and a critical research impetus if the devices are to be deployed routinely for wide-ranging applications.

The method developed here represents a complementary 'class' of bedload estimation to those currently in existence: it is semi-empirical and minimizes the *a priori* assumptions of the model by 'letting the data do the work' in producing bedload estimates. The overarching assumption of the model is that in gravel-bedded rivers impacts detected by a seismic plate are generated by a probabilistic array of *possible* particle sizes in transit, derived from the distribution of bed material grain sizes but constrained by a minimum size detectable by the equipment and a maximum size at the threshold for bedload motion. The approach does not rest on direct calibration with measured sediment loads because it is empirically-attuned by impact count data and thus autogenically-moderated for sediment supply. This produces a supply-limited rather than transport-limited prediction of bedload transport rates, which is far less susceptible to overprediction than sediment transport formulae (Gomez, 2006). The approach is probabilistic in accommodating the inherently stochastic nature of bedload transport and uncertainty-bounded in its accounting for (largely field constrained) variability in model parameterization.

The approach is inherently sensitive to the particle size distribution that represents the domain of detectable sizes. The model is also sensitive to the recording device and its constraints (Downs et al., 2016) and is predicated on the assumption that plate performance is consistent between particle sizes and across different modes of bedload transport (Rickenmann and Fritschi, 2010; Rickenmann and McArdell, 2007; Turowski and Rickenmann, 2009); performance testing of the Benson-type impact plates utilized here is on-going (Benson, pers. comm., 2016). As the model is developed directly from impact count data, we can be fairly confident about the dynamics of, and *relative* rates of, detectable bedload transport indicated by the method. Further investigation of the accordance of (uncertainty-bound) bedload estimates with direct field measurements is recommended under a range of different environmental scenarios and field protocols and to better understand the 'epistemic' uncertainty (see Refsgaard et al., 2007) associated with equipment limitations and model structure/parameterization, but cognizant that such measurements themselves are very error-prone and reveal marked variation between methods (Bunte et al., 2004; Gray 2010a, b; Vericat et al., 2006).

There is considerable potential for the approach to be of benefit to river management projects, for instance in elucidating the geomorphological effectiveness of flows to inform stable channel design (see Soar and Thorne, 2011), and in baseline monitoring of project performance (see Downs et al.,

2011). The model facilitates sensitivity testing of its input parameters, understanding about event-scale bedload dynamics, and longer timeframe installations will provide the basis for understanding bedload sensitivity to hydrological conditions between water years and thus climate change impacts on sediment load, flood risk and aquatic habitats. In demonstrating its proof of concept, this new approach affords a practical and robust method of achieving uncertainty-bound, indicative measures of bedload transport variability and in so doing it contributes to the integration of big data bedload monitoring into a progressive hydrogeomorphic research agenda and the sustainable management of gravel-bed rivers.

Acknowledgements

Data collection was funded by a Seale-Hayne Education Trust grant to the second author. We thank Richard Hartley and Stephen Haley for field assistance, Adrian Simpson and John Hosking for permission to access their lands, Tim Shipley, Sandy Satterly and Andy Roberts for the provision of gauging station data. We are grateful to Dieter Rickenmann and three anonymous reviewers for their constructive comments for improving the manuscript. The impact plates used here are made by Ian Benson (iandesignandbuild@gmail.com).

References

Andrews, E.D., 1983. Entrainment of gravel from naturally sorted riverbed material. Geological Society of America Bulletin 94, 1225. doi:10.1130/0016-7606(1983)94<1225:eogfns>2.0.co;2

Ashmore, P.E., Rennie, C.D., 2012. Gravel-bed rivers: From particles to patterns. Earth Surface Processes and Landforms 38, 217–220. doi:10.1002/esp.3361

Barrière, J., Krein, A., Oth, A., Schenkluhn, R., 2015. An advanced signal processing technique for deriving grain size information of bedload transport from impact plate vibration measurements. Earth Surface Processes and Landforms 40, 913–924. doi:10.1002/esp.3693

Barry, J.J., Buffington, J.M., King, J.G., 2004. A general power equation for predicting bed load transport rates in gravel bed rivers. Water Resources Research 40, W10401. doi:10.1029/2004wr003190

Bathurst, J.C., 2007. Effect of coarse surface layer on bed-load transport. Journal of Hydraulic Engineering 133, 1192–1205. doi:10.1061/(asce)0733-9429(2007)133:11(1192)

Beylich, A.A., Laute, K., 2014. Combining impact sensor field and laboratory flume measurements with other techniques for studying fluvial bedload transport in steep mountain streams. Geomorphology 218, 72–87. doi:10.1016/j.geomorph.2013.09.004

Bogen, J. and Møen, K., 2003, Bedload measurements with a new passive acoustic sensor, in: Bogen, J., Fergus, T., Walling, D. (Eds.), Erosion and Sediment Transport Measurement in Rivers. Technological and Methodological Advances. Proceedings of the Oslo Workshop (19-21 June 2002), IAHS Publication 283, pp. 201-210.

Bravo-Espinosa, M., Osterkamp, W.R., Lopes, V.L., 2003. Bedload transport in alluvial channels. Journal of Hydraulic Engineering 129, 783–795. doi:10.1061/(asce)0733-9429(2003)129:10(783)

Bruner, G., Gibson, S., 2005. Sediment transport modeling in HEC-RAS, in: American Society of Civil Engineers (ASCE) Environmental & Water Resources Institute (EWRI), World Water and Environmental Resources Congress. Anchorage, Alaska, May 5-19, 2005.

Buffington, J.M., Montgomery, D.R., 1997. A systematic analysis of eight decades of incipient motion studies, with special reference to gravel-bedded rivers. Water Resources Research 33, 1993–2029. doi:10.1029/96wr03190

Bunte, K., Abt, S.R., 2001. Sampling surface and subsurface particle-size distributions in wadable gravel- and cobble-bed streams for analysis in sediment transport, hydraulics, and streambed monitoring, General Technical Report RMRS-GTR-74. USDA Forest Service, Rocky Mountain Research Station, Fort Collins, CO, 428 pp.

Bunte, K., Abt, S.R., 2003, Sampler size and sampling time affect bed load transport rates and particle sizes measured with bed load traps in gravel-bed streams, in: Bogen, J., Fergus, T., Walling, D. (Eds.), Erosion and Sediment Transport Measurement in Rivers. Technological and Methodological Advances. Proceedings of the Oslo Workshop (19-21 June 2002), IAHS Publication 283, pp. 126-133.

Bunte, K., Abt, S.R., Potyondy, J.P., Ryan, S.E., 2004. Measurement of coarse gravel and cobble transport using portable bedload traps. Journal of Hydraulic Engineering 130, 879–893. doi:10.1061/(asce)0733-9429(2004)130:9(879)

Bunte, K., Abt, S.R., Potyondy, J.P., Swingle, K.W., 2008. A comparison of coarse bedload transport measured with bedload traps and Helley-Smith samplers. Geodinamica Acta 21, 53–66. doi:10.3166/ga.21.53-66

Bunte, K., Abt, S.R., Potyondy, J.P., Swingle, K.W., 2009. Comparison of three pebble count protocols (EMAP, PIBO, and SFT) in two mountain gravel-bed streams. Journal of the American Water Resources Association 45, 1209–1227. doi:10.1111/j.1752-1688.2009.00355.x

Bunte, K., Abt, S.R., Swingle, K.W., Cenderelli, D.A., 2014. Effective discharge in Rocky Mountain headwater streams. Journal of Hydrology 519, 2136–2147. doi:10.1016/j.jhydrol.2014.09.080

Carling, P.A., 2006. Bedload transport in two gravel-bedded streams. Earth Surface Processes and Landforms 14, 27–39. doi:10.1002/esp.3290140104

Church, M., McLean, D.G., Walcott, J.F., 1987. River bed gravels: sampling and analysis, in: Thorne, C.R., Bathurst, J.C., Hey, R.D. (Eds.), Sediment Transport in Gravel-Bed Rivers. John Wiley & Sons Ltd, Chichester, U.K., pp. 43-87.

Cui, Y., Dusterhoff, S.R., Wooster, J.K., Downs, P.W., 2011. Practical considerations for modeling sediment transport dynamics in rivers, in: Simon, A., Bennett, S.J., Castro, J. (Eds.), Stream Restoration in Dynamic Fluvial Systems: Scientific Approaches, Analyses, and Tools. American Geophysical Union, Washington DC, pp. 503-527

Downs, P.W., Singer, M.S., Orr, B.K., Diggory, Z.E., Church, T.C., 2011. Restoring ecological integrity in highly regulated rivers: The role of baseline data and analytical references. Environmental Management 48, 847–864. doi:10.1007/s00267-011-9736-y

Downs, P.W., Soar, P.J., Taylor, A., 2016. The anatomy of effective discharge: The dynamics of coarse sediment transport revealed using continuous bedload monitoring in a gravel-bed river during a very wet year. Earth Surface Processes and Landforms 41(2), 147–161. doi:10.1002/esp.3785

Ferguson, R.I., 2003. The missing dimension: Effects of lateral variation on 1-D calculations of fluvial bedload transport. Geomorphology 56, 1–14. doi:10.1016/s0169-555x(03)00042-4

Ferguson, R.I., 2005. Estimating critical stream power for bedload transport calculations in gravel-bed rivers. Geomorphology 70, 33–41. doi:10.1016/j.geomorph.2005.03.009

Ferguson, R.I., Paola, C., 1997. Bias and precision of percentiles of bulk grain size distributions. Earth Surface Processes and Landforms 22, 1061–1077. doi:10.1002/(sici)1096-9837(199711)22:11<1061::aid-esp809>3.0.co;2-l

Fritsch, F.N., Carlson, R.E., 1980. Monotone piecewise cubic interpolation. SIAM Journal on Numerical Analysis 17, 238–246. doi:10.1137/0717021

Gomez, B., 2006. The potential rate of bed-load transport. Proceedings of the National Academy of Sciences 103, 17170–17173. doi:10.1073/pnas.0608487103

Gomez, B., Church, M., 1989. An assessment of bed load sediment transport formulae for gravel bed rivers. Water Resources Research 25, 1161–1186. doi:10.1029/wr025i006p01161

Gray, J.R., Laronne, J.B., Marr, J.D.G. (Eds.), 2010a. Bedload-Surrogate Monitoring Technologies. US Geological Survey Scientific Investigations Report 2010–5091. US Geological Survey, Reston, VA.

Gray, J.R., Gartner, J.W., Barton, J.S., Gaskin, J., Pittman, S.A., Rennie, C.D., 2010b. Surrogate technologies for monitoring bed-load transport in rivers, in: Poleto, C., Charlesworth, S.M. (Eds.), Sedimentology of Aqueous Systems. Wiley-Blackwell (an imprint of John Wiley & Sons Ltd), Oxford, U.K., pp. 46–79.

Habersack, H., Seitz, H., Laronne, J.B., 2008. Spatio-temporal variability of bedload transport rate: Analysis and 2D modelling approach. Geodinamica Acta 21, 67–79. doi:10.3166/ga.21.67-79

Han, Z., Chen, G., Li, Y., He, Y., 2015. Assessing entrainment of bed material in a debris-flow event: A theoretical approach incorporating Monte Carlo method. Earth Surface Processes and Landforms 40, 1877–1890. doi:10.1002/esp.3766

Jakeman, A.J., Letcher, R.A., Norton, J.P., 2006. Ten iterative steps in development and evaluation of environmental models. Environmental Modelling & Software 21, 602–614. doi:10.1016/j.envsoft.2006.01.004

Little, C.D., Biedenharn, D.S., 2014. Mississippi River Hydrodynamic and Delta Management study (MRHDM) - Geomorphic assessment. ERDC/CHL Report TR-14-5, United States Army Corps of Engineers, Engineer Research and Development Center, Vicksburg, Mississippi, July 2014, 295 pp.

López, R., Vericat, D., Batalla, R.J., 2014. Evaluation of bed load transport formulae in a large regulated gravel bed river: The lower Ebro (NE Iberian peninsula). Journal of Hydrology 510, 164–181. doi:10.1016/j.jhydrol.2013.12.014

Lisle, T.E., 1995. Particle size variations between bed load and bed material in natural gravel bed channels. Water Resources Research 31, 1107–1118. doi:10.1029/94wr02526

Martin, Y., Ham, D., 2005. Testing bedload transport formulae using morphologic transport estimates and field data: Lower Fraser River, British Columbia. Earth Surface Processes and Landforms 30, 1265–1282. doi:10.1002/esp.1200

Møen, K.M., Bogen, J., Zuta, J.F., Ade, P.K., Esbensen, K., 2010. Bedload measurement in rivers using passive acoustic sensors, in: Gray, J.R., Laronne, J.B., Marr, J.D.G. (Eds)., Bedload Surrogate Monitoring Technologies, US Geological Survey Scientific Investigations Report 2010–5091. US Geological Survey, Reston, VA, pp. 336-351.

Mosley, M.P., Tindale, D.S., 1985. Sediment variability and bed material sampling in gravel-bed rivers. Earth Surface Processes and Landforms 10, 465–482. doi:10.1002/esp.3290100506

Mueller, E.R., Pitlick, J., Nelson, J.M., 2005. Variation in the reference shields stress for bed load transport in gravel-bed streams and rivers. Water Resources Research 41, W04006. doi:10.1029/2004wr003692

Papanicolaou, A.N., Elhakeem, M., Krallis, G., Prakash, S., Edinger, J., 2008. Sediment transport modeling Review - Current and future developments. Journal of Hydraulic Engineering 134, 1–14. doi:10.1061/(asce)0733-9429(2008)134:1(1)

Pitlick, J., Cui, Y., Wilcock, P., 2009. Manual for computing bed load transport using BAGS (Bedload Assessment for Gravel-bed Streams) Software. Gen. Tech. Rep. RMRS-GTR-223. Fort Collins, CO. U.S. Department of Agriculture, Forest Service, Rocky Mountain Research Station. 45 pp.

Recking, A., 2012. Influence of sediment supply on mountain streams bedload transport. Geomorphology 175-176, 139–150. doi:10.1016/j.geomorph.2012.07.005

Recking, A., Liébault, F., Peteuil, C., Jolimet, T., 2012. Testing bedload transport equations with consideration of time scales. Earth Surface Processes and Landforms 37, 774–789. doi:10.1002/esp.3213

Refsgaard, J.C., van der Sluijs, J.P., Højberg, A.L., Vanrolleghem, P.A., 2007. Uncertainty in the environmental modelling process – A framework and guidance. Environmental Modelling & Software 22, 1543–1556. doi:10.1016/j.envsoft.2007.02.004

Reid, I., Frostick, L.E., Layman, J.T., 1985. The incidence and nature of bedload transport during flood flows in coarse-grained alluvial channels. Earth Surface Processes and Landforms 10, 33–44. doi:10.1002/esp.3290100107

Rice, S., Church, M., 1996. Sampling surficial fluvial gravels: The precision of size distribution percentile estimates. Journal of Sedimentary Research 66, 654–665. doi:10.1306/d42683d8-2b26-11d7-8648000102c1865d

Rickenmann, D., In Press. Bedload transport measurements with geophones, hydrophones, and underwater microphones (passive acoustic methods), in: Laronne, J., Tsutsumi, D. (Eds.), Gravel Bed Rivers 8: Gravel Bed Rivers and Disasters. John Wiley & Sons Ltd, Chichester, U.K.

Rickenmann, D., Fritschi, B., 2010. Bedload transport measurements using piezoelectric impact sensors and geophones, in: Gray, J.R., Laronne, J.B., Marr, J.D.G. (Eds)., Bedload Surrogate Monitoring Technologies, US Geological Survey Scientific Investigations Report 2010–5091. US Geological Survey, Reston, VA, pp. 407-423.

Rickenmann, D., McArdell, B.W., 2007. Continuous measurement of sediment transport in the Erlenbach stream using piezoelectric bedload impact sensors. Earth Surface Processes and Landforms 32, 1362–1378. doi:10.1002/esp.1478

Rickenmann, D., McArdell, B.W., 2008. Calibration of piezoelectric bedload impact sensors in the Pitzbach mountain stream. Geodinamica Acta 21, 35–52. doi:10.3166/ga.21.35-52

Rickenmann, D., Turowski, J.M., Fritschi, B., Klaiber, A., Ludwig, A., 2012. Bedload transport measurements at the Erlenbach stream with geophones and automated basket samplers. Earth Surface Processes and Landforms 37, 1000–1011. doi:10.1002/esp.3225

Rickenmann, D., Turowski, J.M., Fritschi, B., Wyss, C., Laronne, J., Barzilai, R., Reid, I., Kreisler, A., Aigner, J., Seitz, H., Habersack, H., 2014. Bedload transport measurements with impact plate geophones: Comparison of sensor calibration in different gravel-bed streams. Earth Surface Processes and Landforms 39, 928–942. doi:10.1002/esp.3499

Rustomji, P., Wilkinson, S.N., 2008. Applying bootstrap resampling to quantify uncertainty in fluvial suspended sediment loads estimated using rating curves. Water Resources Research 44, W09434. doi:10.1029/2007WR006088

Ryan, S.E., Porth, L.S., 1999. A field comparison of three pressure-difference bedload samplers. Geomorphology 30, 307–322. doi:10.1016/s0169-555x(99)00059-8

Shields, A., 1936. Anwendung der Aehnlichkeitsmechanik und der turbulenzforschung auf die geschiebewegung [Application of similarity principles and turbulence research to bed-load movement]. Mitteilung der Preussischen versuchsanstalt fuer Wasserbau und Schiffbau, Heft 26, Berlin. Translation by Ott, W.P. and van Uchelin, J.C., Hydrodynamics Laboratory Publication 167, US Soil Conservation Service Cooperative Laboratory, California Institute of Technology, Pasadena, California.

Sterling, S.M., Church, M., 2002. Sediment trapping characteristics of a pit trap and the Helley-Smith sampler in a cobble gravel bed river. Water Resources Research 38, 19–.1–19.11. doi:10.1029/2000wr000052

Soar, P.J., Thorne, C.R., 2011. Design discharge for river restoration, in: Simon, A., Bennett, S.J., Castro, J.M. (Eds.), Stream Restoration in Dynamic Fluvial Systems: Scientific Approaches, Analyses, and Tools. Geophysical Monograph Series 194. American Geophysical Union, Washington, DC, pp. 123-149. doi: 10.1029/2010GM001009

Tsakiris, A.G., Papanicolaou, A.N., Lauth, T.J., 2014. Signature of bedload particle transport mode in the acoustic signal of a geophone. Journal of Hydraulic Research 52, 185–204. doi:10.1080/00221686.2013.876454

Turowski, J.M., Badoux, A., Rickenmann, D., 2011. Start and end of bedload transport in gravel-bed streams. Geophysical Research Letters 38, L04401. doi:10.1029/2010gl046558

Turowski, J.M., Rickenmann, D., 2009. Tools and cover effects in bedload transport observations in the Pitzbach, Austria. Earth Surface Processes and Landforms 34, 26–37. doi:10.1002/esp.1686

Turowski, J.M., Rickenmann, D., 2011. Measuring the statistics of bed-load transport using indirect sensors. Journal of Hydraulic Engineering 137, 116–121. doi:10.1061/(asce)hy.1943-7900.0000277

Uusitalo, L., Lehikoinen, A., Helle, I., Myrberg, K., 2015. An overview of methods to evaluate uncertainty of deterministic models in decision support. Environmental Modelling & Software 63, 24–31. doi:10.1016/j.envsoft.2014.09.017

Vericat, D., Batalla, R.J., 2010. Sediment transport from continuous monitoring in a perennial Mediterranean stream. Catena 82, 77–86. doi:10.1016/j.catena.2010.05.003

Vericat, D., Church, M., Batalla, R.J., 2006. Bed load bias: Comparison of measurements obtained using two (76 and 152 mm) Helley-Smith samplers in a gravel bed river. Water Resources Research 42, W01402. doi:10.1029/2005wr004025

Vázquez-Tarrío, D., Menéndez-Duarte, R., 2015. Assessment of bedload equations using data obtained with tracers in two coarse-bed mountain streams (Narcea river basin, NW Spain). Geomorphology 238, 78–93. doi:10.1016/j.geomorph.2015.02.032

Wallerstein, N. (Ed.), 2006. Accounting for Sediment in Rivers: A Tool Box of Sediment Transport and Transfer Analysis Methods and Models to Support Hydromorphologically-Sustainable Flood Risk Management in the UK. Flood Risk Management Research Consortium, Research Report UR9. United Kingdom, 130 pp.

Warrick, J.A., 2015. Trend analyses with river sediment rating curves. Hydrological Processes 29(6), 936–949. doi:10.1002/hyp.10198

Whitaker, A.C., Potts, D.F., 2007. Coarse bed load transport in an alluvial gravel bed stream, Dupuyer Creek, Montana. Earth Surface Processes and Landforms 32, 1984–2004. doi:10.1002/esp.1512

Wilcock, P.R., 2001. Toward a practical method for estimating sediment-transport rates in gravel-bed rivers. Earth Surface Processes and Landforms 26, 1395–1408. doi:10.1002/esp.301

Wolman, M.G., 1954. A method of sampling coarse river-bed material. Transactions, American Geophysical Union 35(6), 951–956. doi:10.1029/tr035i006p00951

Wyss, C.R., Rickenmann, D., Fritschi, B., Turowski, J.M. Weitbrecht, V., Boes R.M., 2014. Bedload grain size estimation from the indirect monitoring of bedload transport with Swiss plate geophones at the Erlenbach stream, in: Schleiss, A.J., Cesare, G. de, Franca, M.J., Pfister, M. (Eds.), River Flow 2014: Proceedings of the International Conference on Fluvial Hydraulics, Lausanne, Switzerland (3-5 September). CRC Press/Balkema, Leiden, The Netherlands, pp. 1907-1912.

Wyss, C.R., Rickenmann, D., Fritschi, B., Turowski, J.M., Weitbrecht, V., Boes, R.M., 2016a. Measuring bed load transport rates by grain-size fraction using the Swiss plate geophone signal at the Erlenbach. Journal of Hydraulic Engineering 142(5). doi:10.1061/(asce)hy.1943-7900.0001090

Wyss, C.R., Rickenmann, D., Fritschi, B., Turowski, J.M., Weitbrecht, V., Boes, R.M., 2016b. Laboratory flume experiments with the Swiss plate geophone bed load monitoring system: 1. Impulse counts and particle size identification. Water Resources Research 52, 7744–7759. doi:10.1002/2015wr018555

Wyss, C.R., Rickenmann, D., Fritschi, B., Turowski, J.M., Weitbrecht, V., Travaglini, E., Bardou, E., Boes, R.M., 2016c. Laboratory flume experiments with the Swiss plate geophone bed load monitoring system: 2. Application to field sites with direct bed load samples. Water Resources Research 52, 7760–7778. doi:10.1002/2016wr019283

Zingg, T., 1935. Beiträge zur Schotteranalyse. Schweizerische Mineralogische und Petrologische Mitteilungen 15, 39-140.